2014

REEVALUATION OF THE AAPM TG-43 BRACHYTHERAPY DOSIMETRY PARAMETERS FOR AN ^{125}I SEED, AND THE INFLUENCE OF EYE PLAQUE DESIGN ON DOSE DISTRIBUTIONS AND DOSE-VOLUME HISTOGRAMS

Prakash Aryal
University of Kentucky, prakash@uky.edu

STUDENT AGREEMENT:

I represent that my thesis or dissertation and abstract are my original work. Proper attribution has been given to all outside sources. I understand that I am solely responsible for obtaining any needed copyright permissions. I have obtained needed written permission statement(s) from the owner(s) of each third-party copyrighted matter to be included in my work, allowing electronic distribution (if such use is not permitted by the fair use doctrine) which will be submitted to UKnowledge as Additional File.

I hereby grant to The University of Kentucky and its agents the irrevocable, non-exclusive, and royalty-free license to archive and make accessible my work in whole or in part in all forms of media, now or hereafter known. I agree that the document mentioned above may be made available immediately for worldwide access unless an embargo applies.

I retain all other ownership rights to the copyright of my work. I also retain the right to use in future works (such as articles or books) all or part of my work. I understand that I am free to register the copyright to my work.

REVIEW, APPROVAL AND ACCEPTANCE

The document mentioned above has been reviewed and accepted by the student's advisor, on behalf of the advisory committee, and by the Director of Graduate Studies (DGS), on behalf of the program; we verify that this is the final, approved version of the student's thesis including all changes required by the advisory committee. The undersigned agree to abide by the statements above.

Prakash Aryal, Student

Dr. Janelle A. Molloy, Major Professor

Dr. Tim Gorringe, Director of Graduate Studies

REEVALUATION OF THE AAPM TG-43 BRACHYTHERAPY DOSIMETRY PARAMETERS FOR AN ^{125}I SEED, AND THE INFLUENCE OF EYE PLAQUE DESIGN ON DOSE DISTRIBUTIONS AND DOSE-VOLUME HISTOGRAMS

DISSERTATION

A dissertation submitted in partial fulfillment of the
requirements for the degree of Doctor of Philosophy in the
College of Arts and Sciences
at the University of Kentucky

By
Prakash Aryal
Lexington, Kentucky

Director: Janelle A. Molloy, PhD, Associate Professor of Radiation Medicine

Lexington, Kentucky

Co-Director: Mark J. Rivard, PhD, Professor, Tufts University

Boston, Massachusetts

2014

ABSTRACT OF DISSERTATION

REEVALUATION OF THE AAPM TG-43 BRACHYTHERAPY DOSIMETRY PARAMETERS FOR AN ^{125}I SEED, AND THE INFLUENCE OF EYE PLAQUE DESIGN ON DOSE DISTRIBUTIONS AND DOSE-VOLUME HISTOGRAMS

The TG-43 dosimetry parameters of the Advantage^{TM} ^{125}I model IAI-125A brachytherapy seed were studied. An investigation using modern MCNP radiation transport code with updated cross-section libraries was performed. Twelve different simulation conditions were studied for a single seed by varying the coating thickness, mass density, photon energy spectrum and cross-section library. The dose rate was found to be 6.3% lower at 1 cm in comparison to published results. New TG-43 dosimetry parameters are proposed.

The dose distribution for a brachytherapy eye plaque, model EP917, was investigated, including the effects of collimation from high-*Z* slots. Dose distributions for 26 slot designs were determined using Monte Carlo methods and compared between the published literature, a clinical treatment planning system, and physical measurements.

The dosimetric effect of the composition and mass density of the gold backing was shown to be less than 3%. Slot depth, width, and length changed the central axis (CAX) dose distributions by < 1% per 0.1 mm in design variation. Seed shifts in the slot towards the eye and shifts of the ^{125}I-laden silver rod within the seed had the greatest impact on the CAX dose distribution, changing it by 14%, 9%, 4.3%, and 2.7% at 1, 2, 5, and 10 mm, respectively, from the inner scleral surface.

The measured, full plaque slot geometry delivered 2.4% $\pm$ 1.1% higher dose along the plaque's CAX than the geometry provided by the manufacturer and 2.2%±2.3% higher than Plaque Simulator^{TM} (PS) treatment planning software (version 5.7.6). The D_{10} for the simulated tumor, inner sclera, and outer sclera for the measured slot plaque to manufacturer provided slot design was 9%, 10%, and 19% higher, respectively. In comparison to the measured plaque design, a theoretical plaque having narrow and deep slots delivered 30%, 37%, and 62% lower D_{10} doses to the tumor, inner sclera, and outer sclera, respectively. CAX doses at –1, 0, 1, and 2 mm were also lower by a factor of 2.6, 1.72, 1.50, and 1.39, respectively. The study identified substantial sensitivity of the EP917 plaque dose distributions to slot design.

KEYWORDS: Monte Carlo methods, dosimetry, ^{125}I, TG-43, eye plaque brachytherapy

Prakash Aryal,

_____
Student's signature

Date 04/16/2014

REEVALUATION OF THE AAPM TG-43 BRACHYTHERAPY DOSIMETRY PARAMETERS FOR AN ^{125}I SEED, AND THE INFLUENCE OF EYE PLAQUE DESIGN ON DOSE DISTRIBUTIONS AND DOSE-VOLUME HISTOGRAMS

By

Prakash Aryal

Janelle A. Molloy, Ph.D.

(Director of Dissertation)

Mark J. Rivard, Ph.D.

(Co-Director of Dissertation)

Tim Gorringe, Ph.D.

(Director of Graduate Studies)

April 16, 2014

Dedicated to my parents

Mr. Purna Prasad Aryal and Mrs. Durga Kumari Aryal

ACKNOWLEDGEMENTS

This Ph.D. dissertation has not been possible without the help and support of many individuals who are involved directly or indirectly for many years.

First and foremost, I would like to express my deepest and sincere gratitude to my advisor Dr. Janelle A. Molloy for her tireless constant encouragement, guidance, and support. Her great strengths on critical thinking, organizational skill, and analytical interpretation of the results have made great impact on me. I am honored to have such a wonderful advisor. This dissertation would not have been possible without her outstanding contribution.

I am very indebted to my co-advisor Dr. Mark J. Rivard for his great effort, guidance, and support to complete this work. His contribution for ^{125}I seed, and EP917 plaque modeling, and data analysis was priceless. His tireless guidance, constant inspiration, suggestions and support made this difficult task a reality. I am extremely proud to have him as my co-advisor of my dissertation.

My sincere gratitude also goes to Dr. Ali S. Meigooni for inspiring me to work on curvilinear source model. His contribution and constant support to this work was invaluable.

I am also very thankful to Dr. Joseph Brill, chairman of my advisory committee, for his continuous support, encouragement and suggestions. His continuous support during these years has been very appreciable.

I would like to thank Dr. Ellis Johnson, a committee member, for discussion and suggestion of this work.

I would like to thank other committee members Dr. Tim Gorringe, Dr. Steven Yates for their valuable suggestions. A special thank goes to Dr. William St. Clair for serving as my outside examiner and providing suggestions and ideas to my dissertation. I also want to thank Dr. Bishnu Thapa, and Dr. Ganesh Narayanasamy for related discussion to my dissertation.

I would also like to thank Dr. Marcus Randall, chairman of department of radiation medicine for providing me a PC for my research work. His continuous support of my higher education was very valuable.

I am very grateful to Dr. Robert Zwicker for inspiring me to pursue my Ph.D. at University of Kentucky. His support was very appreciable.

I would also like to thank faculty and staff of radiation medicine department for their support and valuable discussion over the years.

I would like to thank my daughter Samichhya and son Prashanta for their love and support. They were less demanding for the time they needed during all these years.

I am very grateful and thankful to my parents Purna P. Aryal, and Durga K. Aryal for their continuous love, support, and encouragement during this long journey. It is unthinkable without their continuous love and support.

I am also thankful to my father in-law Krishna Bilas Adhikari and mother in-law Hari Maya Adhikari for their inspiration, and support to complete this task.

Thanks go to my sisters Bishwa K. Aryal, and Sunita Mishra and brother Bishwa P. Aryal for their continuous support and encouragement.

A sincere gratitude goes to my brother in laws Kishor Dutta Mishra, and Kalyan Adhikari for their inspiration and support.

I would also like to thank my nieces Anuja Poudel, and Manju Pandey for constant support and encouragement.

Lastly, very special thanks go to my wife Sita K. Aryal. This work would not have been possible without her continuous love, help and support. Her patience, inspiration, and motivation have made this task reach a successful conclusion.

TABLE OF CONTENTS

LIST OF TABLES

LIST OF FIGURES

CHAPTER 1 INTRODUCTION

1.1 General Introduction

A tumor can be benign or malignant. Cancer is a type of tumor characterized by overgrowth of abnormal cells which grow by dividing to make new cells. Their ability to metastasize distinguishes them from other tumor cells. There are many different types of cancer and each is unique in how it grows and responds to treatment. One way to stop the cancer from growing is to interfere with the cancer cell's ability to multiply. Radiation, used at high doses, causes changes in the cancer cell that affect the ability to reproduce and eventually leads to cell death.

Low energy photons (e.g., 20 keV to 150 keV) can be used for the diagnosis of patient disease or for the treatment of cancerous tumor, while high energy photons (e.g., 1 MeV to 20 MeV) are used to kill cancer cells. Radiation therapy, like surgery, chemotherapy and biological therapy, is one modality to treat cancer. The radiation can come from radioactive substances or linear accelerators. The treatment of cancer by linear accelerators is termed external beam radiation therapy, while treatment of cancer by encapsulated radioactive substances (sources) is called brachytherapy. A patient may receive radiation therapy in conjunction with other cancer treatment but more than half of the patients with cancer receive radiation therapy either by external beam radiation therapy or brachytherapy or both.[1]

Brachytherapy is a treatment modality using encapsulated sealed radiation sources. The treatment is given by placing the sources directly into the tumor volume or close to the tumor volume. There are two types of radionuclide sources used in brachytherapy. The first type is short lived with low energy. These radionuclides,

including ^{125}I, ^{103}Pd, and^{131}Cs, are used to treat cancer by placing them in the tumor volume permanently. The second type of radionuclide is long lived sources with higher energy. These radionuclides including ^{137}Cs, ^{60}Co, and ^{192}Ir are used for temporary brachytherapy implants. Most brachytherapy treatments are from photon emitting radionuclides; however beta and neutron emitting radionuclides are also used.

Brachytherapy can be used for many types of cancer. Some common cancers treated with brachytherapy include prostate, breast, lung, esophageal, gynecologic, anal/rectal, sarcomas, eye as well as head and neck.[2] Low dose rate (LDR) brachytherapy treatment uses low strength radioactive sources[3]. The treatment time is normally longer and is most commonly used to treat prostate and gynecological cancers. The practice in brachytherapy has been changed with the advancement of technology and imaging modalities for target localization, and for planning and optimizing the proposed geometry. Figure 1.1 shows imaging modalities used for LDR prostate brachytherapy and Figure 1.2 shows an LDR prostate treatment plan using ultrasound imaging.

Figure 1.1 Imaging modalities used for prostate LDR brachytherapy.

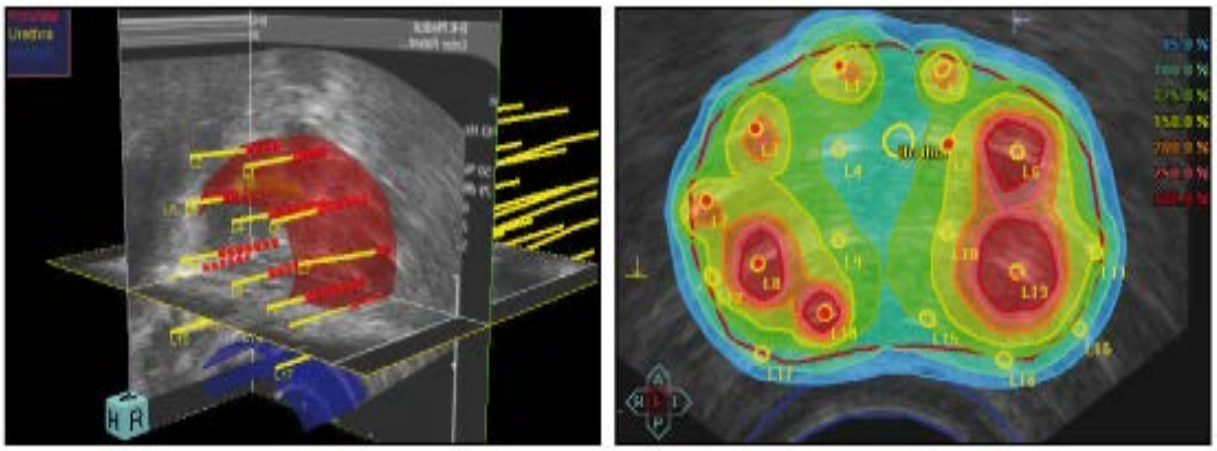

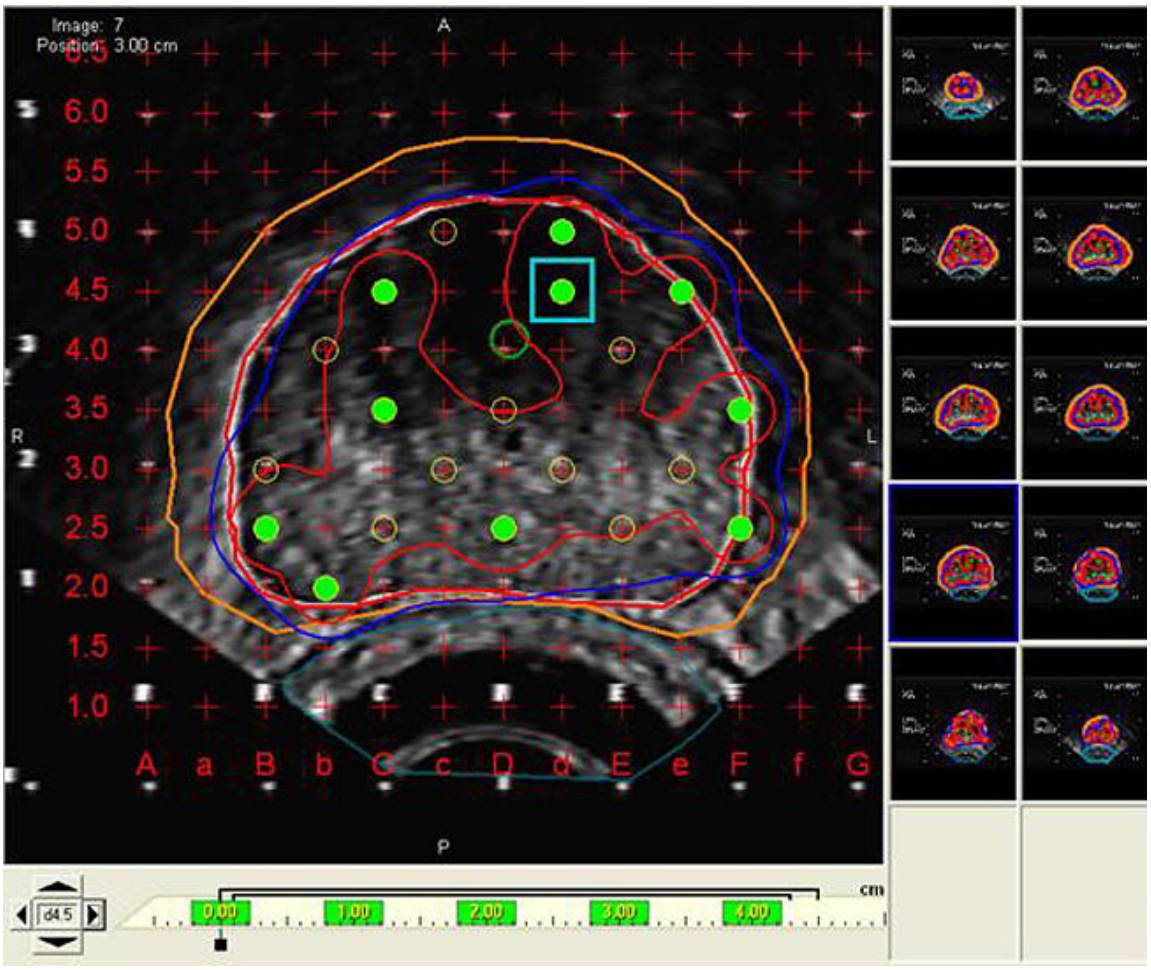

Figure 1.2 Ultrasound image used for prostate LDR brachytherapy computerized treatment planning.

High dose rate (HDR) brachytherapy treatment uses high strength (e.g., 10 Ci) radioactive sources contained within an after loading device. The designated catheters and transfer guide tubes are attached to applicators and the HDR unit. The applicators are placed in the patient during patient simulation. The unit can be operated to send an active radioactive source wire to catheters which are attached to the applicator devices to deliver the radiation dose to the tumor. The source remains for short periods of time in each position based on the treatment plan produced. HDR treatment usually takes 5-20 minutes for most of the gynecological cancers.

HDR treatment has become popular for delivering the desired radiation dose to the tumor in just a few minutes. This may also be a comfort to patients who, in some cases, require less hospitalization. However; multiple treatments are required to reduce the radiation toxicity to normal tissues. Figure 1.3 shows two HDR brachytherapy units.

Figure 1.3 HDR after loader units. The unit on the left is from Nucletron™ (Netherlands) and on the right is the unit from Varian Medical Systems™ (California, USA)

1.2 Motivation

Many authors have independently characterized various low-energy; commercially produced brachytherapy sources.[12,13,18,19,53] ^{125}I radioactive seed has been widely used for permanent brachytherapy. The dosimetry of these low energy sources is well documented in AAPM task group reports published in 1995, 2004, and 2007.[4,5,14]

The dose calculation is determined with dosimetry parameters such as air-kerma strength, dose rate constant, radial dose function, geometry function, and anisotropy function as described in series of AAPM task group (TG) 43 reports. However, one method used to calculate these consensus dosimetric parameter values was based on a previous Monte Carlo algorithm. The algorithm has been revised and updated since the publication of these AAPM reports in 2004 and 2007.[4,5] But the consensus data for low energy photon emitting radionuclides has yet to be reviewed based on the updated methodology. Therefore, one motivation of this project is to obtain the values of dosimetric parameters in the TG-43 reports.[4,5,14] Of the ^{125}I seed models, the IsoAid Advantage I-125™ Seed (model IAI-125A), was selected for this study.

Intraocular tumors have been treated for many years with ^{125}I brachytherapy. Different gold eye plaques with silastic inserts for the ^{125}I seeds are now available commercially. These Collaborative Ocular Melanoma Study (COMS) plaques come with various circular diameter sizes 8 mm, 12 mm, 14 mm, 18 mm, and 22 mm. COMS plaques with notches are used to limit the dose to critical structures. However, these plaques are not suitable to treat elongated and asymmetrical superficial ocular tumors. These superficial ocular tumors are normally 1 mm to 5 mm deep. Moreover, these are associated with uncertainties with seed carriers (silastic). Therefore, researchers at the University of Southern California (USC) designed a plaque to overcome these issues. This study is focused on the elongated EP917 (USC #9) plaque where radioactive seeds are embedded directly in to the slots of the plaque. The radiation dose tolerance of superficial eye structures such as the sclera has also been an issue. Therefore, this study also focuses on reconstructing the EP917 plaque and quantifying the effect of attenuation and back scatter from the gold backing and its collimation.

1.3 Proposed Study

The consensus data of TG-43 parameters are based on Monte Carlo (MC) calculations and experimental methods.[4,5,14] Most brachytherapy treatment planning systems have adopted the TG-43 formalism. The MCNP5 code for radiation transport simulation has been revised and updated to include photon cross section libraries, variance reduction techniques and other improvements since its original publication in 1987. But we continued to rely on outdated consensus data in which the brachytherapy treatment planning systems are commissioned for brachytherapy dose calculation. Therefore, the principal aim of this study is to determine and investigate dosimetric parameters of the TG-43 report with revised and updated Monte Carlo version 5 (MCNP5) dose calculation algorithm for an ^{125}I seed (model IAI-125A). The seed was fully modeled, redesigned and thoroughly investigated. In our study, we incorporated the most recent manufacturer's seed information and previous authors' early works. All AAPM TG-43 reports recommendations were also properly followed.

1.4 Dissertation Outline

The dissertation consists of five chapters. In Chapter 1, a brief overview of cancer, radiation therapy, and brachytherapy is discussed. Chapter 2 presents the interaction of radiation with matter, an introduction of Monte Carlo simulations, and brachytherapy radiation dose calculation methods. Chapter 3 presents the investigation of TG-43 dosimetry parameters for a particular model of ^{125}I seed including the recommendation to use our new proposed dosimetry parameters. The contents of this chapter were published in *Medical Physics*.[65] In this work, the source characteristics of ^{125}I (model IAI-125A), MC simulation techniques, calculation of TG-43 dosimetry parameters, and an uncertainty analysis are described. Chapter 4 provides independent

dosimetric assessment of the model EP917 episcleral brachytherapy plaque. The contents of this chapter have also been submitted to *Medical Physics*. This chapter includes experimental validation of published plaque design as well as an assessment of variations in single slot and full plaque designs using MC methods. The dosimetric influence of these variations on tumor and sclera are presented. Chapter 5 presents a summary and conclusions.

CHAPTER 2 THEORETICAL BACKGROUND

2.1 Radiation Interactions with Matter

^{125}I emits characteristic X-rays (3.77 keV to 31.704 keV) and gamma rays (35.49 keV). The photons in general are indirect ionizing radiation and undergo Rayleigh scattering, as well as the photoelectric effect, Compton scattering, and pair production interaction processes to transfer their energy to the medium. Photoelectric effect and Compton scattering interactions are the most dominant radiological interactions in brachytherapy.

2.1.1 Raleigh (coherent) Scattering

Raleigh scattering occurs when the photon interacts with the entire atom. This process is also called Coherent scattering. This is an elastic interaction and the photon does not lose energy. In this process, the atom oscillates in phase due to the electromagnetic wave energy of the incident photon. The photon energy absorbed induces a vibration of the atom. The vibrating atom then de-excites and emits an equivalent amount of energy. The photon is scattered with a small angle, and in a slightly different direction but with same wavelength. No ionization occurs in this interaction since electrons have not been ejected from an atom. Figure 2.1 shows the Raleigh scattering process.[6]

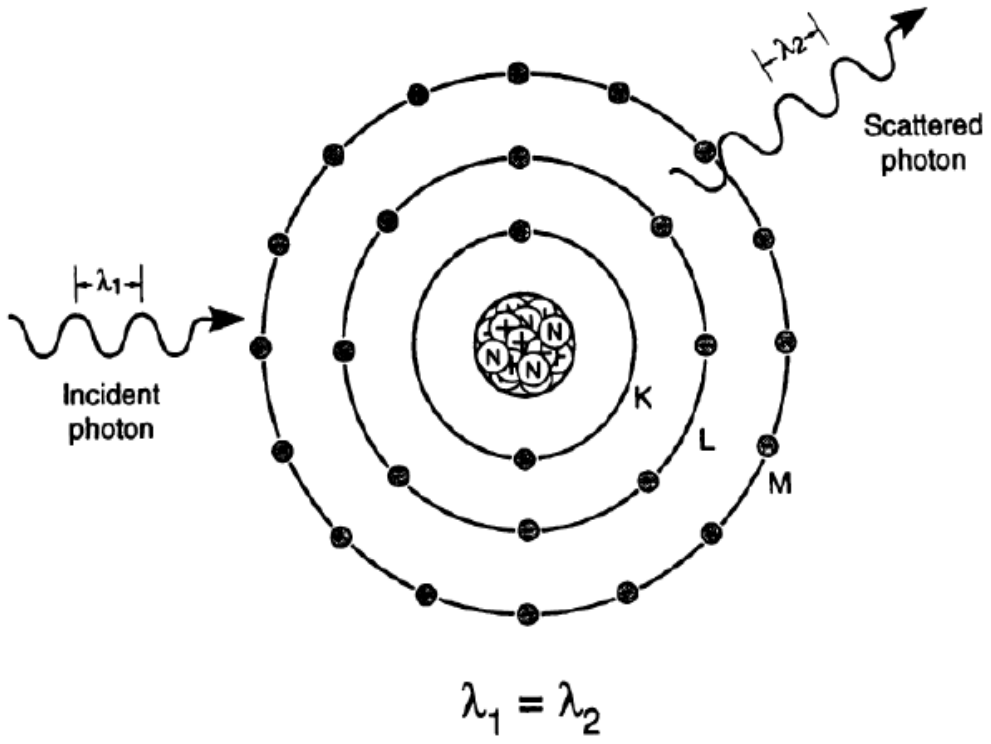

Figure 2.1 Rayleigh scattering process. The incident photon with wavelength λ_1 interacts with an atom. The scattered photon with wavelength λ_2 is emitted with approximately same wavelength and energy. Courtesy from J.T. Bushberg et. al.

The momentum is also conserved in this process. The cross-section per atom in this process is given by:[7]

$$\sigma_{a,R} \approx \left(\frac{Z}{h\nu}\right)^2 \left(cm^2/_{atom}\right) \tag{2.1}$$

The equation (2.1) can be multiplied by number of atoms per gram to obtain the macroscopic cross-section and is given by:

$$\frac{\sigma_R}{\rho} \approx = \frac{z}{h\upsilon^2}\left(cm^2/g\right) \tag{2.2}$$

Therefore, the macroscopic cross-section per unit mass is directly proportional to atomic number of an atom and inversely proportional to square of the energy of the photon. Raleigh scattering occurs at very low energies and there is no energy transferred to the medium. As such, this process has no role in radiation dosimetry.[7]

2.1.2 Photoelectric Effect

In the photoelectric process, the incident photon interacts with a tightly bound, inner shell electron (usually the K shell) of an atom. The photon is completely absorbed and an electron (called photoelectron) is emitted with kinetic energy (E_e) equal to the photon energy, (E_0=hv), minus the orbital binding energy (E_b) assuming that kinetic energy imparted to the recoiling atom is nearly zero.

$$E_e = E_0 - E_b \tag{2.3}$$

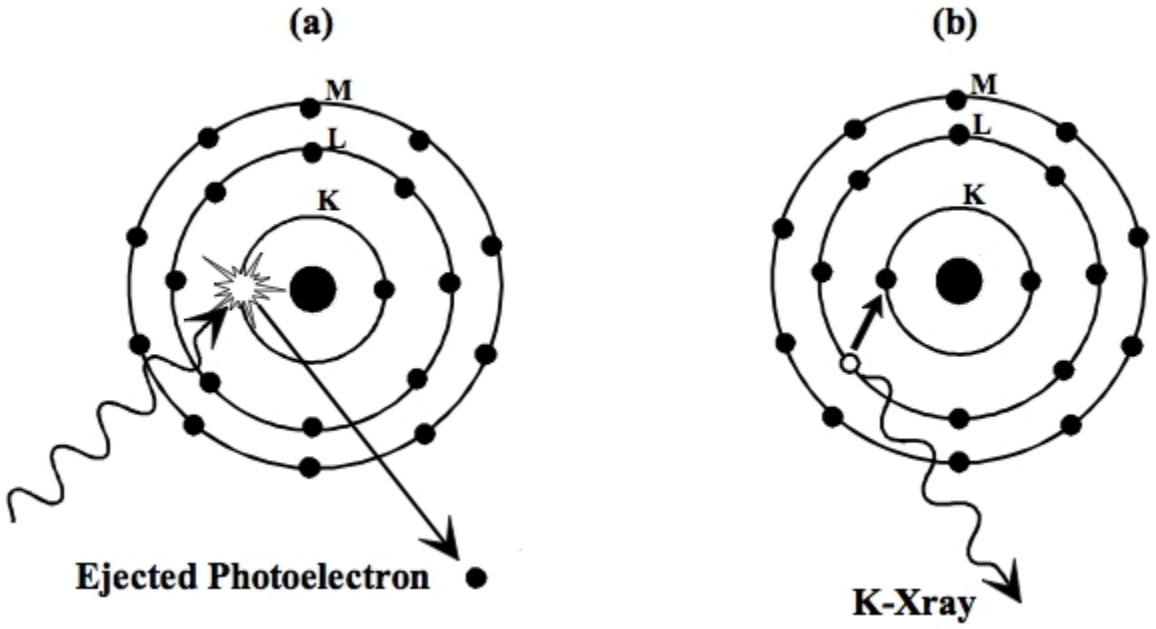

Figure 2.2 Photoelectric interaction processes. In the photoelectric process, the incident x-ray photon collides with a low energy (in this case, K-shell) orbital electron and transfers all of its energy to that electron. The photoelectric event is followed by a subsequent cascade of electron transitions from higher- to lower energy orbitals to fill the vacated positions, which results emission of characteristic radiation (en.wikibooks.org).

The photoelectric process occurs when the incident photon energy is greater than the binding energy of the orbital electron. The vacancy created by the ejected electron is filled by the higher orbital electrons. The probability of a photoelectric interaction depends on the medium and photon energy. The photoelectric cross-section per atom is given by

$$\sigma_\tau = \frac{32}{3}\sqrt{2\pi}r_e^2\,\acute{\alpha}^4 Z^5\left(\frac{m_e c^2}{E_0}\right)^{\frac{7}{2}} \qquad (2.4)$$

(Fundamentals of PET SPECT M. Wernick, J. Aarsvold, 2004)

Where $32/3\sqrt{2\pi}r_e^2\,\acute{\alpha}^4$ is a constant of proportionality, r_e is the classical electron radius, Z is the atomic number of the medium, and E_0 is the energy of incident photon. When

E_0 is near K, L, M shell binding energy, the equation (2.4) needs to be multiplied by correction factor $(1/Z^2)(m_ec^2/E_0)^{1/2}$ to accounts for quantum effects. This increases the cross-section near $E_0 = E_b$ which creates sharp discontinuity called absorption edge.

Therefore, $$\sigma_\tau \propto \frac{Z^3}{E_0^4} \quad (2.5)$$

Photoelectric absorption is a dominant interaction for low energy photons (keV) and high atomic number materials. The probability of photoelectric interaction decreases with increasing photon energy. Sharp discontinuities called absorption edges exist for high Z materials like titanium, silver, and gold (Figure 2.4). The probability of interaction is greater for photons with energies just above the absorption edge than those with energies just slightly below the edge.

2.1.3 Compton (incoherent) Scattering)

Compton scattering is inelastic or non-classical scattering, and is the predominant interaction for brachytherapy radiation in tissue. In this process, the incident photon interacts with energy , E_γ, greater than the binding energy of a loosely bound outer shell electron.

$$E_\gamma = E_{\gamma'} + E_{e^-} \quad (2.6)$$

Here E_γ is the incident energy of the photon, $E_{\gamma'}$ is the energy of scattered photon, and E_{e^-} is the energy of an ejected electron.

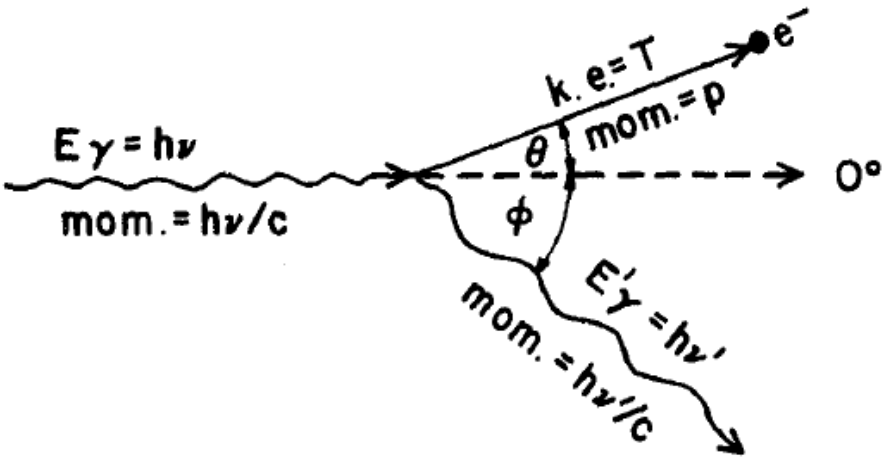

Figure 2.3 *The Compton scattering process, where, the incident photon is scattered by a free electron at an angle ϕ. The Compton electron carries energy T in its direction of scatter by an angle θ. Energy and momentum are conserved in the interaction.* [7]

The energy of the scattered photon is given by:[7]

$$h\nu' = \frac{h\nu}{1 + \frac{h\nu}{m_0 c^2}(1 - \cos\phi)} \tag{2.7}$$

The kinetic energy of the recoil electron is T= $h\nu - h\nu'$. The electron is ejected at an angle, θ

$$\cot\theta = \left(1 + \frac{h\nu}{m_0 c^2}\right) \tan\left(\phi/2\right) \tag{2.8}$$

Where ϕ is the angle of the scattered photon.The binding energy of the ejected electron is comparatively small and can be ignored for the range of energy used in our study.

2.1.4 Processes Relevant to the Current Work

Most of the photon emitting brachytherapy sources emit poly-energic spectra in the range of 21 keV to 662 keV. The mean energy of the spectrum emitted by the ^{125}I radioactive seed model used in this study is about 28 keV. Therefore, photoelectric and Compton are the two primary, relevant interactions mechanisms that we considered.

To illustrate the relative importance of the potential interaction mechanisms, we present Fig. 2.4, which displays the linear attenuation coefficients for the media used in this study. Data are displayed over the range of 1 keV to 100 keV. The photoelectric effect dominates at energies below 26 keV in soft tissue, while Rayleigh scattering contributes only 5% to 10% at this energy. When higher energy photons interact with a low Z material (e.g., tissue), Compton scattering becomes dominant. The low energy photons from ^{125}I produce short range electrons, therefore, can be ignored. The collision kerma approximates the absorbed dose. The pair production interaction has a minimum energy of 1.02 MeV and as such, is not relevant within the context of this study.

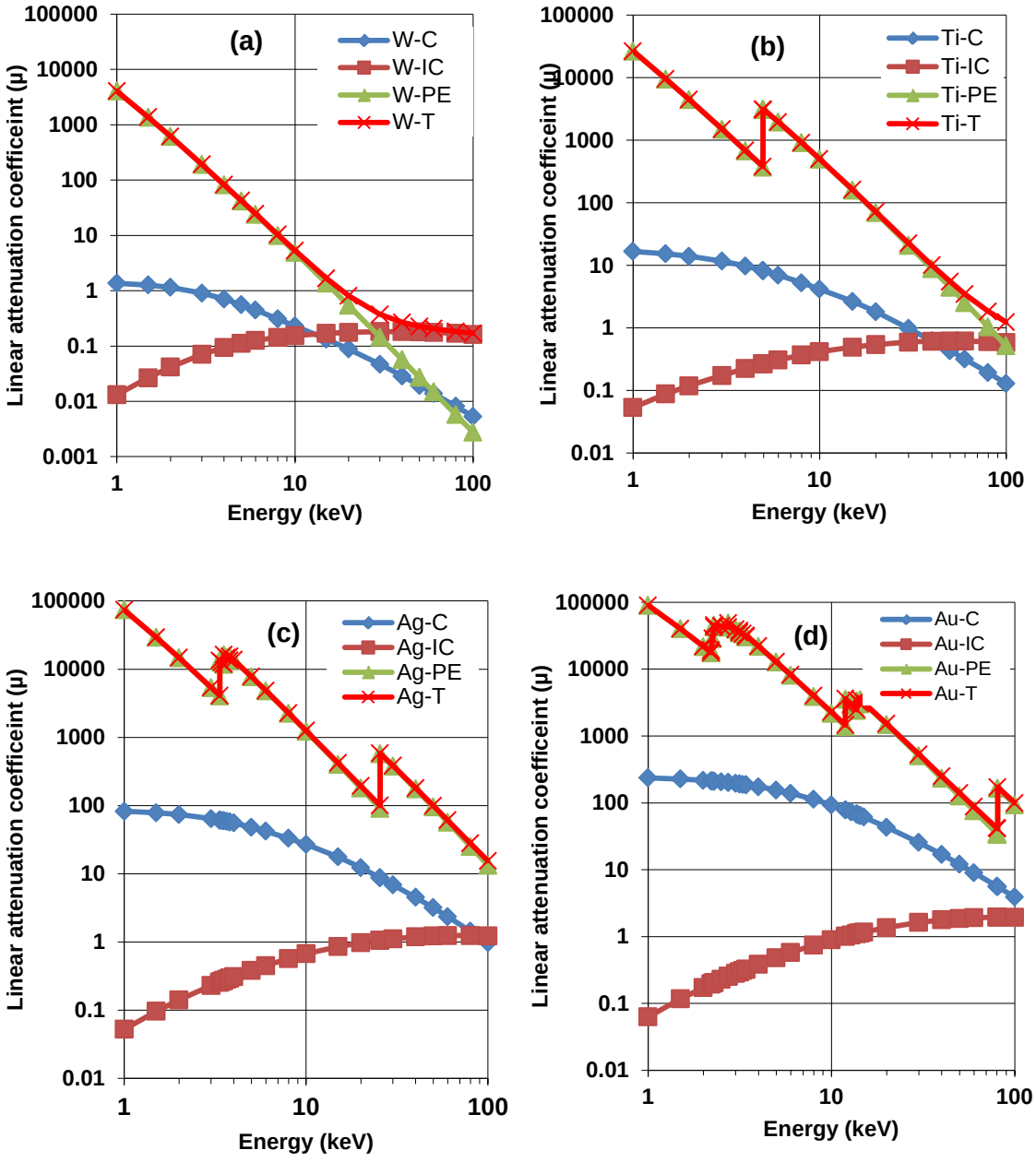

Figure 2.4: Coherent, incoherent, photoelectric, and total linear attenuation coefficients for (a) water, (b) titanium, (c) silver, and (d) gold as a function of energy. The asorption edges (the discrete increase in attenuation coefficients) occur due to photoelectric absorption when photon energy exceeds the binding energy of inner shell electrons (K, L, M…) thus increasing number of electrons available for interaction. This effect is significant for high Z material for low energy range(like energy from ^{125}I).

2.2 Monte Carlo Simulation

The Monte Carlo N-Particle version 5 (MCNP5) is a radiation transport code that is widely used to simulate the behavior of radiation particles based on the random statistical nature of their histories. It is a process that simulates transport of photons, electrons, neutrons, and other particles into a selected media where the nature of interaction of these particles can be estimated. MCNP5 is particularly useful for complex problems that cannot be modeled by computer codes that use deterministic methods. The individual probabilistic events that comprise a process are simulated sequentially. An input file is created which can be read by the MCNP5 code. It includes cell cards, surface cards, the description of materials, and selection of cross-sections. The input file also includes tallies desired for calculation, and variance reduction techniques to improve efficiency. It is good practice to benchmark and validate the given simulations using other MC codes and/or measurements. The MCNP5 code performs checks to ensure that problem geometries, materials, and sources are self-consistent throughout the input file.

Due to the equivalence between collision kerma and absorbed dose in the energy range (<300 keV), it is not necessary to simulate the electron histories. Therefore, we only used photon treatment simulation mode (MODE P) in all simulations.

The general MCNP5 simulation process is given by the following flow chart

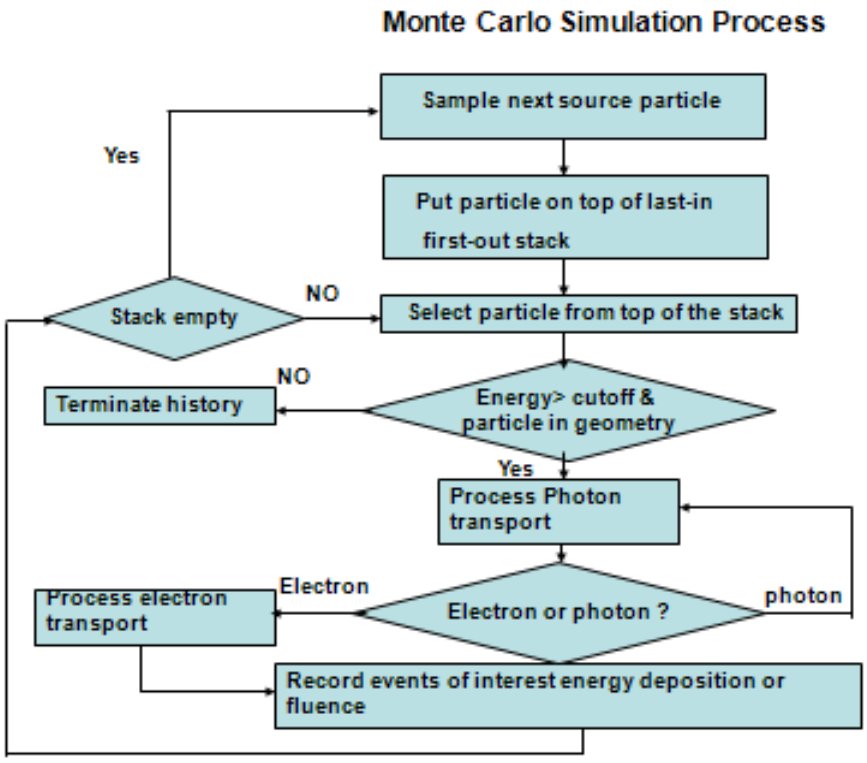

Figure 2.5: Monte Carlo simulation process flow chart. The particle is selected from top of the stack. If the energy is greater than cutoff energy (<5 keV) it goes through photon transport process and records event if electron is ejected. If photon is ejected it goes through series of iteration process until it further ejects electron and records the event.

2.2.1 Physics of MCNP5

The physics of the MCNP5 simulation code is based on the interaction of neutrons, photons, or electrons. Photoatomic and photonuclear are the two interactions included in MCNP5. These relate to elemental and isotropic aspects, respectively. The cross-sectional data of these events are stored in tables separately. The directory file (XSDIR) is created for each data table and users can select a specific data table by assigning the atomic number Z, mass number A, and library specifier ID in the form ZAID.[8]

The Evaluated Nuclear Data File (ENDF) system and the Evaluated Photon Data Library (EPDL) provide the primary sources of nuclear data. [9] MCNP5 contains nuclear data tables for neutrons, photons, electrons and neutron-induced photon interactions. Photon and electron data are mostly atomic in nature but photonuclear data are also included in MCNP5.

There are two physics photon interaction models used in MCNP5, simple, and detail. The simple model ignores Raleigh scattering and fluorescent photons from photoelectric absorption. Therefore, this model is designed for high-energy photon problems where contribution from photoelectric effect is insignificant. This physics model uses implicit capture but can be overridden with the CUT:P card.

The detail physics model accounts for fluorescent photons and also includes Raleigh scattering after photoelectric absorption. The electron binding effects are accounted for by using Compton profiles and form factors. Analog capture is always used. The detailed physics treatment uses energy below 100 MeV. All the photon emitting brachytherapy sources fall into the detail physics treatment category.

The electrons produced from photons are handled in three ways; (1) electron transport mode turned on (Mode P E), in this case all the photon collisions except Raleigh (coherent) scatter can create electrons that are stored for later transport; (2) electron transport mode turned off (Mode P). If a particle which has weight W and energy E makes a track length or segment T within a specified cell volume, V, then the segment makes a contribution WTE/V to the energy flux (fluence) to cell. The sum of the contributions is reported as the *F4 tally in the MCNP output. If $\psi(\vec{r}, \mathrm{E}, \Omega, \mathrm{t})$ represents the angular fluence distribution, then *F4 represents the physical quantity

$$^{*}\,\mathrm{F4} = \frac{\mathrm{WTE}}{\mathrm{V}} = \frac{1}{\mathrm{V}} \int dt \int_{\mathrm{V}} \mathrm{dV} \int_{\mathrm{E}} \mathrm{dE} \int_{4\pi} \mathrm{d}\Omega \, E \, \psi(\vec{r}, \mathrm{E}, \Omega, \mathrm{t}) \tag{2.9}$$

2.3 TG-43 Dosimetry Formalism Algorithms

Previous formalisms introduced inconsistencies and uncertainties in dose calculation due to variability in encapsulation or internal structure. Moreover, these formalisms were based on apparent activity, equivalent mass of radium, exposure rate constants, and tissue attenuation coefficients. Older formalisms were based on photon fluence around the source in free space which ignored scattering medium. Accurate modeling of the anisotropy effect and dose determination in a scattering medium of brachytherapy sources is almost impossible from the distribution of photon fluence in free space.[10]

The TG-43[14] formalism allows two-dimensional dose calculation by introducing the following dosimetric parameters air-kerma strength, dose-rate constant, radial dose function, geometry function, and anisotropy function. The last two parameters are a function of distance and angle. For cylindrically symmetric sources, the two-dimensional dose rate in a polar coordinate system is given by

$$\dot{D}(\mathrm{r}, \theta) = S_K . \Lambda . \frac{\mathrm{G_L}(\mathrm{r}, \theta)}{\mathrm{G_L}(r_0, \theta_0)} . \mathrm{g_L}(\mathrm{r}) . \mathrm{F}(\mathrm{r}, \theta) \tag{2.10}$$

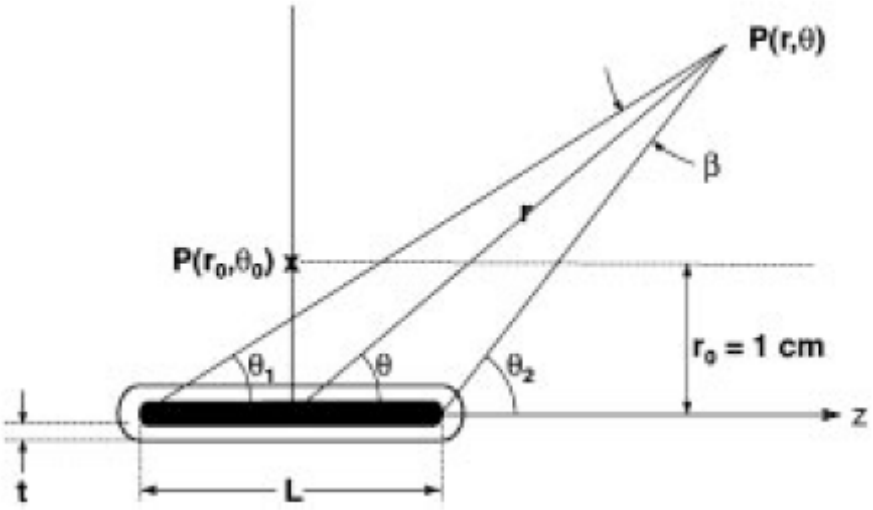

Figure 2.6 Coordinate system used for brachytherapy dosimetry calculations.

2.3.1 Air-Kerma Strength,S_K

The air-kerma strength, S_K, is a measure of the strength of a brachytherapy source and is specified in terms of air-kerma rate at a calibration point along the transverse axis of the source. It is the product of air-kerma rate,$\dot{K}_\delta$, in *vacuo* and the square of the distance, *d*.

$$S_K = \dot{K}_\delta\,(d)d^2 \qquad (2.11)$$

The calibration distance must be large enough that the source may be treated as a point source. The air kerma rate is measured with the Wide Angle Free Air Chamber (WAFAC).[11] The measured air-kerma rate is corrected for photon attenuation and scattering in air and any medium between the source and the detector. The low energy, $\delta(< 5keV)$, photons originating from the outer layer of the steel or titanium source cladding is excluded because it does not contribute significant dose beyond 0.1 cm in

tissue. But low energy 3.77 keV of ^{125}I is included for eye plaque simulations since sclera of the eye is just a millimeter thick.

2.3.2 Dose-Rate Constant, Λ

The dose-rate constant is defined as the ratio of the dose rate at 1 cm on the transverse plane in water a 15 cm radius phantom and the air kerma strength.

$$\Lambda = \frac{\dot{D}(r_0, \theta_0)}{S_K} \tag{2.12}$$

The dose-rate constant depends on source model and the radionuclide and is influenced by source geometry, encapsulation, self-filtration, and the spatial distribution of radioactivity within the source.[14]

2.3.3 Geometry Function, G(*r*,*θ*)

The geometry function provides an effective inverse square law correction based upon an approximate model of the spatial distribution of radioactivity within the source and ignores the photon absorption and scattering within the source. It is the interpolation between points of calculated or measured dose rates which provides for approximations with sufficient accuracy in treatment planning applications. However, the three dimensional distribution of the density of radioactivity of many sources is uncertain.[10] Therefore, the geometry function is explicitly given assuming a point or line source approximation as recommended by TG-43.

$$G_P(r, \theta) = r^{-2} \qquad \text{point} - \text{source approximation} \tag{2.13}$$

$$G_L(r,\theta) = \begin{cases} \dfrac{\beta}{Lr\sin\theta} \; if \; \theta \neq 0° \\ \left(r^2 - {L^2}/{4}\right)^{-1} \; if \; \theta = 0° \end{cases} \quad \text{Line source approximation} \qquad (2.14)$$

Where β $(= \theta_2 - \theta_1)$ is the angle in radians subtended by the tips of the hypothetical line source with respect to the calculation point. The geometry function used to calculate radial dose and two dimensional anisotropy functions when deriving dose rates, should use identical parameters including active length, L.

2.3.4 Radial Dose Function, $g_X(r)$

The radial dose function, $g_X(r)$ accounts for dose fall off on the transverse plane due to scattering and attenuation of photon fluence in a water medium. It is expressed by the following equation

$$g_X(r) = \frac{\dot{D}(r,\theta_0)}{\dot{D}(r_0,\theta_0)} \frac{G_X(r_0,\theta_0)}{G_X(r,\theta_0)} \qquad (2.15)$$

The subscript "X" indicates whether a point source, "P", or line source, "L" approximation is used. In the present study, a line source approximation is used for all Monte Carlo simulations.

A fifth order polynomial fit to the data is also useful as a means to efficiently evaluate for any general position, r.

$$g_X(r) = a_0 + a_1 r + a_2 r^2 + a_3 r^3 + a_4 r^4 + a_5 r^5 \qquad (2.16)$$

Where a_0 through a_5 are constants. These constants should be determined and fit the data for a treatment planning application over an acceptable range.

2.3.5 Two-Dimensional (2D) Anisotropy Function, *F*(*r*,*θ*)

The anisotropy function describes the variation of dose as a function of polar angle with respect to the transverse plane. The 2D anisotropy function is small at smaller polar angles and reaches unity at $90°$.

$$F(r,\theta) = \frac{\dot{D}(r,\theta)}{\dot{D}(r,\theta_0)} \frac{G_L(r,\theta_0)}{G_L(r,\theta)} \tag{2.17}$$

The large dose gradient near the radioactive sources makes it difficult to measure dose rates at distances less than 0.5 cm. The Monte Carlo calculation method is more reliable in estimating dose rates at shorter distances (<1 cm).[14]

The 2D anisotropy function decreases as (1) radial distance, r, decreases, (2) as θ approaches $0°$ or $180°$, (3) as encapsulation thickness increases, (4) as photon energy decreases. The same active length,L should be used to evaluate $G_L(r,\theta)$ and to extract $g_L(r)$, and $F(r,\theta)$ from dose distribution.

Some of the clinical treatment planning systems have adopted a one-dimensional anisotropy approach. This ignores the orientation of the longitudinal axis of the source and simplifies by approximating the complex two dimensional distributions. The 1D anisotropy factor, $\phi_{an}(r)$ is expressed as

$$\phi_{an}(r) = \frac{\int_0^{\pi} \dot{D}(r,\theta) \sin(\theta)\, d\theta}{2\dot{D}(r,\theta_0)} \tag{2.18}$$

Therefore, this 1D anisotropy factor $\phi_{an}(r)$ is the ratio of dose rate at distance r, averaged with respect to solid angle, to the dose rate on the transverse plane is at the same distance. Equation (2.11) can be written as

$$\dot{D}(r) = S_K . \Lambda . \frac{G_L(r,\theta)}{G_L(r_0,\theta_0)} . g_L(r) . \phi_{an}(r) \qquad (2.19)$$

CHAPTER 3 A MODERN MONTE CARLO INVESTIGATION OF THE TG-43 DOSIMETRY PARAMETERS FOR AN ^{125}I SEED ALREADY HAVING AAPM CONSENSUS DATA

3.1 Introduction

The Advantage^{TM125}I model IAI-125A brachytherapy seed (IsoAid LLC, Port Richey, FL) has been available for clinical use since 2000. In 2002, Solberg *et al*.[12] and Meigooni *et al*.[13] published the TG-43[14] dosimetry parameters for this seed using both measurement and Monte Carlo (MC) calculation methods for radiation transport simulations. The methodology to prepare American Association of Physicists in Medicine (AAPM) consensus values for TG-43 dosimetry parameters are derived by taking the combined results from MC calculations and TLD measurements.[15] Given the data in these two publications and the need for uniform clinical practice, the AAPM approved posting of this seed on the joint AAPM/Radiological Physics Center (RPC) Registry of Brachytherapy Sources on July 14, 2002.

In 2004, the AAPM published a task group report (TG-43U1)[15] update to the 1995 TG-43 report[14] to recommend improved dosimetry methods and dosimetric characterization of low-energy photon-emitting brachytherapy seeds. A 2007 supplement AAPM report (TG-43U1S1)[16] included additional seeds such as the model IAI-125A seed. AAPM consensus data used for the model IAI-125A seed was based on the results from Solberg *et al*. and Meigooni *et al*. as these publications met the AAPM dosimetric prerequisites. The line-source radial dose function $g_L(r)$ with an active length of 0.3 cm, the 2D anisotropy function $F(r, \theta)$, and 1D anisotropy function $\phi(r)$ were directly taken from Solberg *et al*. MC results, while the consensus value for the dose-rate constant Λ was taken as the average value from Solberg *et al*. and Meigooni *et al*. results using MC and experimental methods.

Over the past decade, the MC radiation transport codes used in preparation of some AAPM consensus datasets have been revised. For example, Solberg *et al.* used the MCNP4C code with photoelectric cross-section data from Berger and Hubbell, while Meigooni *et al*. used the PTRAN code with the DLC 99 (data library code-99) photon cross-section library.[17] In 2003, the MCNP5 code was released and included improved photon interaction modeling and cross-section libraries. Moreover, 04p cross-section library provided more data points between the energy range (10 keV to 80 keV) than 02p cross-section.[50]

In 2008, Taylor and Rogers calculated TG-43 parameters for the model IAI-125A seed using the modified EGSnrc user-code called BrachyDose,[18] and obtained Λ values 4.0% and 5.9% lower than published by Solberg *et al*. and Meigooni *et al*., respectively. Further, Taylor and Rogers obtained $g_L(r)$ values differing by greater than 10% from Solberg *et al*. or Meigooni *et al*.

The model 6711 ^{125}I seed (Oncura, Arlington Heights, IL), has a similar design to the model IAI-125A seed. In 2010, Kennedy *et al*.[19] reported using the MCNP5 code for simulating the model 6711 seed and reported a Λ value 6.2% lower than the 2007 AAPM TG-43U1S1 report consensus. [16] Due to the similarities of 6711 and IAI-125A we would expect to see similar differences in obtaining dose rate constant (DRC) using updated MCNP5 vs current consensus DRC data.

These inconsistencies in the dosimetry parameters in the literature and with the AAPM consensus data are important, and prompted investigation on the potential causes for these differences. The current study proposes a new reference dosimetry dataset, compares this dataset to the published literature, and examines the sensitivity

of radiation transport simulation results for the model IAI-125A seed to variations in MC source modeling data.

3.2 Methods and Materials

Accurate MC simulations of brachytherapy seeds require knowledge of the physical properties of the source. This includes the dimensions of all materials as well as their compositions and densities. Some aspects are well understood through the manufacturing process such as the length, thickness, and diameter of the source capsule and internal components such as a radiopaque marker. However, other aspects may not be well known such as the thickness and mass density of the radioactive coating of the radiopaque marker.

3.2.1 Source Characteristics Model IAI-125A Seed

The model IAI-125A seed consists of a silver rod (right cylinder) contained within a titanium capsule (4.54 g/cm^3) with dimensions specified in Table 1. The capsule is filled with argon gas at an assumed mass density of 1.662 mg/cm^3. These source characteristics were confirmed with the manufacturer and through external dimensional measurements of radioactive seeds in a manner similar to Rivard *et al*.[20]

All rod surfaces are uniformly coated with a silver iodide mixture. Following review of the literature and discussion with the manufacturer, the coating thickness is not well documented. Solberg *et al*. did not report the thickness, although private communication indicated that a thickness of 0.5 μm was simulated. Meigooni *et al*. assumed a thickness of 1 μm. Both thicknesses were used for creation of the

consensus data recommended in the 2007 AAPM TG-43U1S1 report,[16] but the manufacturer recently informed us that 0.5 μm is more realistic. Therefore, the IAI-125A seed was simulated using a variety of coating thicknesses (i.e., 0.1 μm, 0.5 μm, 1 μm, and 2 μm) to investigate the influence of coating thickness variations on dosimetry parameters. Two coating densities (4.93 g/cm^3 and 6.003 g/cm^3)[13,21] were considered based on variations used in the literature, where the latter value is considered more representative of the manufactured product.

For benchmarking the simulations and quantitative comparisons due to its similar design, TG-43 parameters for the model 6711 ^{125}I seed were compared to those for the model IAI-125A ^{125}I seed. The dimensions are also included in Table 3.1. Nominal dimensions of the model IAI-125A seed and a schematic diagram depicting a cross-sectional display as examined under the MC simulation conditions is shown in Figure 3.1.

Table 3.1 Dimensional characteristics for the model IAI-125A and model 6711 ^{125}I seeds (all dimensions are given in millimeters).

Parameter	model IAI-125A	model 6711
Ag rod length	3.00	2.80
Ag rod bevel at 45°	0.00	0.05
Ag rod diameter	0.50	0.50
Capsule outer length	4.50	4.55
Capsule inner length	3.70	3.75
Capsule outer diameter	0.80	0.80
Capsule inner diameter	0.70	0.66
Capsule endweld thickness	0.35	0.40

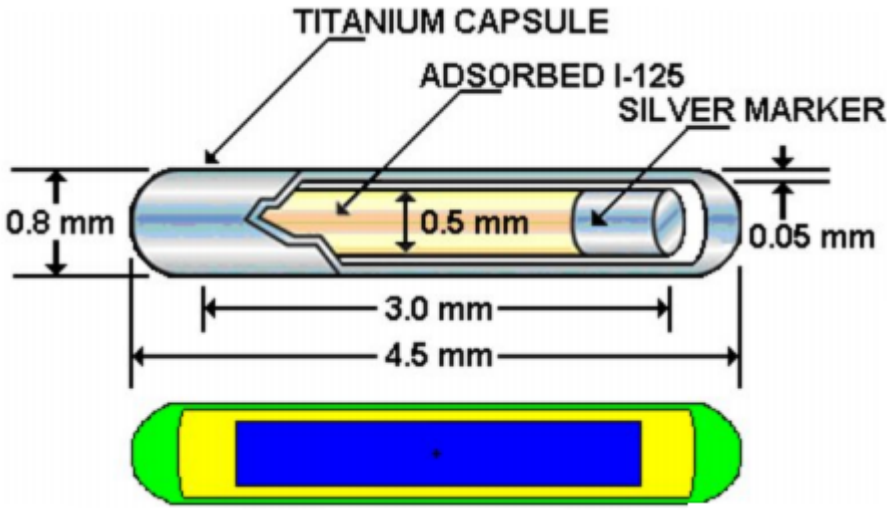

Figure 3.1 Schematic diagram of the model IAI-125A seed. The top image shows nominal seed dimensions as specified by the manufacturer instructions for use. The bottom image shows the proposed standard seed geometry from the MCNP5 visual editor output.

3.2.2 Monte Carlo Simulations

The MCNP5 radiation transport code was used for dosimetry simulations.[22] The MCNP5 default photon cross-section library, MCPLIB04 (04p), was applied for benchmarking. The older MCPLIB02 (02p) cross-section library was used for comparison to the Solberg *et al*. and Meigooni *et al.* results. Based on the range of secondary charged particles, simulations considered only photon transport. The ^{125}I photon energy spectra in Table 2 were taken from Solberg *et al*., and the National Nuclear Data Center (NNDC).[12,23,24] The NNDC-based photon energy spectra were taken as our proposed standard for comparison as it is more recent than that used by Solberg *et al*., and the AAPM has recently recommended that NNDC spectra data be reference data.[25]

The seed was centrally positioned within a 20 cm radius water sphere having a mass density of 0.998 g/cm^3.[26] This volume was divided into a contiguous sampling space bounded by spheres and conics as similar to the geometry used by Rivard for another ^{125}I seed.[27] A 5 keV cutoff energy was used for dose-rate calculations using a track-length estimator under the assumption of equivalence of absorbed dose to collisional kerma.

Table 3.2 ^{125}I disintegration photon energy spectra as used in the simulations. Note that the provided NNDC-based spectrum[23,24] excludes photons < 5 keV (i.e., 3.77 keV line), and is normalized to unity for comparison with that of Solberg et al.[12]

Solberg *et al*.		NNDC-based	
Energy [keV]	Intensity [photons / history]	Energy [keV]	Intensity [photons / history]
22.1	0.14		
25.0	0.04		
27.4	0.64	27.202	0.27730
		27.472	0.51172
		30.944	0.04723
31.1	0.14	30.995	0.09128
		31.704	0.02628
35.5	0.04	35.4922	0.04619
27.4 (mean)	1.00	28.36 (mean)	1.00000

Twelve input simulation files were created in water and in vacuum to model the IAI-125A seed with different coating thicknesses and mass densities, photon cross section libraries, and photon spectra. These simulation conditions are listed in Table 3.3. Simulation condition 11 was proposed as an updated standard because it has the most recent information on source design (coating thickness and density), cross-section library, and photon energy spectrum. Results of TG-43 dosimetry parameters from simulation condition 11 were compared to those obtained by Solberg *et al*., Meigooni *et al*., Taylor and Rogers, and Kennedy *et al*. Further, results from all 12 simulation

conditions were intercompared to determine the sensitivity of dosimetry results to each variable.

Table 3.3 Simulation conditions used for MC modeling. Simulation condition 11 is proposed for determination of a new reference dosimetry data. The DLC-99 cross-section library by Meigooni et al. and the XCOM cross-section library by Taylor and Rogers may be considered equivalent to the 02p and 04p cross-section libraries available within the MCNP code, respectively.

Investigator	Coating thickness [µm]	Coating density [g/cm^3]	Cross-section library	Photon energy spectrum	Endweld thickness [mm]
Solberg *et al*.	0.5	10.48	02p	S	0.24
Meigooni *et al*.	1.0	6.003	DLC-99	M	0.10
Taylor and Rogers	1.0	6.003	XCOM	TG-43U1	0.10
Kennedy *et al*.	1.75	6.20	04p	TG-43U1	0.40
Simulation condition 1	0.1	4.93	02p	S	0.35
Simulation condition 2	0.5	4.93	02p	S	0.35
Simulation condition 3	2.0	4.93	02p	S	0.35
Simulation condition 4	0.1	4.93	04p	S	0.35
Simulation condition 5	0.5	4.93	04p	S	0.35
Simulation condition 6	2.0	4.93	04p	S	0.35
Simulation condition 7	0.5	4.93	04p	N	0.35
Simulation condition 8	0.5	6.003	02p	N	0.35
Simulation condition 9	1.0	6.003	02p	N	0.35
Simulation condition 10	1.0	6.003	04p	N	0.35

Simulation condition 11	0.5	6.003	04p	N	0.35
Simulation condition 12	0.5	6.003	04p	S	0.35

For spectrum choice, M= MIRD pamphlet 10,[28] N = NNDC-based,[24] TG-43U1=Rivard *et al.*[15]and S = Solberg *et al*.[12]

3.2.3 TG-43 Dosimetry Parameters

For MC simulations of air-kerma strength s_K, the seed was positioned in vacuum and the photon energy fluence was estimated $\pm$ 7.6° from the transverse plane to mimic the sampling geometry of the Wide Angle Free Air Chamber (WAFAC) at the National Institute of standards and Technology (NIST).[29] A thin vacuum shell (0.00002 mm) at distance of 30 cm was created in order to score air kerma rate. In combination with the dose rate in water on the transverse plane at r = 1 cm, Λ was derived according to the approach described by Rivard.[27] For all simulations in water, the phantom geometry and sampling space was the same as that of Rivard.[27]Values for $g_L(r)$, $F(r,\theta)$, and $\phi(r)$ were determined over the same range as that by Rivard.[27] A total of 10^{10} and 10^9 particle histories were used to assure minimal statistical uncertainties for vacuum and water calculations, respectively. Specifically, the Type A uncertainties (k=1 coverage factor) were 0.02% at r = 1 cm and 0.03% at r = 5 cm in water, and 0.02% at 30 cm in vacuum for calculation of s_K

3.2.4 Uncertainty Analysis

As recommended in the 2004 AAPM TG-43U1 report, a dosimetric uncertainty analysis was performed to determine the uncertainties associated with each component

of the MC simulation process. The uncertainties presented in Table 3.4 are based on the similar methods as used by Rivard,[27]and following the 2012 AAPM TG-138 report guidelines for specifying brachytherapy dosimetric uncertainties where a *k*=1 coverage factor is provided.[30] The uncertainty components were derived as follows

(a) Due to the similar design with the model 6711 ^{125}I seed, the dosimetric uncertainties for $\dot{d}_{(1,\theta_0)}$, $\dot{d}_{(5,\theta_0)}$, and s_K, were taken from Rivard.[27] For the dose-rate at 1 cm, this 0.3% value also matched that of Kennedy *et al*. These uncertainties canceled out for derivation of Λ and $g_L(5)$ uncertainties.

(b) Many brachytherapy seeds exhibit dynamic internal components, see for example Refs. 31 and 32. From the central position, the Ag rod in the model IAI-125A seed can move laterally within the titanium capsule interior by a maximum of 0.01 cm. Assuming a rectangular distribution for this motion and dose changes attributed to changes in solid-angle, this results in uncertainties of 0.58%, 0.12%, and 0.19% for $\dot{d}_{(1\text{ cm},\theta_0)}$, $\dot{d}_{(5\text{ cm},\theta_0)}$, and s_K, respectively. These uncertainties combined in quadrature for derivation of Λ and $g_L(5)$ uncertainties.

(c) Rivard *et al*.[23] compared different ^{125}I photon energy spectra to determine their dosimetric influence. Subsequently, a new data evaluation for the ^{125}I photon energy spectrum following nuclear disintegration was performed by Katakura in 2011.[33] Upon comparison of this more recent data to the prior evaluation by Katakura in 1999,[34] and with removal of the 3.77 keV photon from both spectra, the mean photon energy changed from 28.3644 keV to 28.3676 keV, respectively. Utilizing the 1999 and 2011 spectra in calculations of $\dot{d}_{(1,\theta_0)}$,

$\dot{d}_{(5,\theta_0)}$, and s_K, the dosimetric uncertainties were 0.03%, 0.01%, and 0.04%, respectively. While these uncertainties canceled out for the derivation of $g_L(5)$, they combined in quadrature for the derivation of Λ for an uncertainty of 0.05%.

(d) The 2004 AAPM TG-43U1 report provides recommended compositions and mass densities for water and air. Simplifying this as 0.1% uncertainty in the mass density of the material, the estimated uncertainties (k=1) of $\dot{d}_{(1,\theta_0)}$, $\dot{d}_{(5,\theta_0)}$, and s_K were 0.05%, 0.23%, and 0.002%, respectively. These uncertainties combined in quadrature for the derivation of Λ and $g_L(5)$.

(e) Rivard *et al*.[23] compared three different MC codes and found the dosimetric influence on $\dot{d}_{(1,\theta_0)}$, $\dot{d}_{(5,\theta_0)}$, and s_K for a point ^{125}I source to be about 0.1% (k=1). This value was used herein for the model IAI-125A ^{125}I seed simulations. These uncertainties canceled out for the derivation of Λ and $g_L(5)$ uncertainties.

(f) Using the PENELOPE MC code, Andreo *et al*.[35]calculated the Type B uncertainties for μ_{en}/ρ in water and air between 1 keV to 2 MeV. In water at 24.6 keV and 34.1 keV, Andreo *et al*. obtained standard (k=1) uncertainties of 0.82% and 0.66%, respectively. At r = 1 cm and r = 5 cm, the mean photon energy in water for the current study was about 27.30 keV and 27.17 keV, respectively, corresponding to μ_{en}/ρ Type B uncertainties of 0.771% and 0.773%, respectively. In air at 24.6 keV and 34.1 keV, Andreo *et al*. obtained standard (k=1) uncertainties of 0.76% and 0.62%, respectively, which gave a μ_{en}/ρ Type B uncertainty of 0.715% at the mean photon energy in vacuum at r = 30 cm. The methods of Andreo *et al*. had statistical uncertainties of 0.07% (k=1). These

uncertainties combined in quadrature for derivation of Λ, but canceled out for the derivation of $g_L(5)$ uncertainties.

(g) The uncertainties in μ/ρ are estimated to be slightly less than the uncertainty in μ_{en}/ρ.[36] Using a value of 0.6%, the resultant uncertainties on $\dot{d}_{(1,\theta_0)}$, $\dot{d}_{(5,\theta_0)}$, and s_K were 0.28%, 1.40%, and 0% (due to vacuum), respectively. These uncertainties combined in quadrature for derivation of Λ and $g_L(5)$ uncertainties.

(h) The sampling voxels at 1 cm and 5 cm in water were 0.002 cm and 0.1 cm, respectively, while the sampling voxel at 30 cm in vacuum was 0.02 μm thick. This resulted in tally volume averaging uncertainties of 0.0001%, 0.01%, and < 0.0000001% for $\dot{d}_{(1,\theta_0)}$, $\dot{d}_{(5,\theta_0)}$, and s_K, respectively. These uncertainties combined in quadrature for derivation of Λ and $g_L(5)$ uncertainties.

(i) Photon histories totaling 10^9 and 10^{10} were used for simulations in water and vacuum, respectively. This gave k=1 statistical uncertainties of 0.02%, 0.03% at 1 cm and 5 cm in water, respectively. For s_K, the k=1 statistical uncertainty was 0.02%. These uncertainties combined in quadrature for the derivation of Λ and $g_L(5)$ uncertainties.

Overall, the standard uncertainty for the TG-43 dosimetry parameters Λ and $g_L(5)$ were 1.2% and 1.6%, respectively, and were dominated by the μ_{en}/ρ and μ/ρ uncertainties. Some uncertainty components (such as the source capsule geometry and the physics model used in the MC code) cancelled out for Λ and thus had lower overall uncertainty than the uncertainty for the ratio of $\dot{d}_{(1,\theta_0)}/s_K$. This reduction in the overall

uncertainty was also true for the derivation of $g_L(5)$ where additional components that canceled out included the source photon spectrum and μ_{en}/ρ.

Table 3.4 Dosimetric uncertainty analysis of uncertainty components for MC simulations of the model IAI-125A. The statistical (Type A) and non-statistical (Type B) uncertainty components are expressed as percentages and are due to random and systematic effects, respectively.

	$\dot{d}_{(1,\theta_0)}$		s_K		Λ		$\dot{d}_{(5,\theta_0)}$		$g_L(5)$	
Uncertainty component										
	Type A (%)	Type B (%)	Type A (%)	Type B (%)	Type A (%)	Type B (%)	Type A (%)	Type B (%)	Type A (%)	Type B (%)
Source capsule geometry		0.3		0.2		---		0.2		---
Dynamic internal components		0.58		0.02		0.58		0.12		0.59
Source photon spectrum		0.03		0.04		0.05		0.01		---
Phantom composition		0.05		0.002		0.05		0.23		0.24
Physics of MC code		0.1		0.1		---		0.1		---
μ_{en}/ρ for dose calculation	0.07	0.771	0.07	0.715	0.10	1.05	0.07	0.773	---	---
μ/ρ for phantom attenuation		0.28		0		0.28		1.40		1.43

Tally volume averaging		0.0001		0.00001		0.0001		0.01		0.01
Tally statistics	0.02		0.02		0.03		0.03		0.04	
Quadrature sum	0.07	1.05	0.07	0.75	0.10	1.23	0.08	1.64	0.04	1.56
Total standard uncertainty		1.06		0.75		1.24		1.64		1.56

3.3 Results

3.3.1 s_K

The s_K values decreased with increasing coating thickness for both cross-section libraries. Relative to the proposed standard value of a 0.5 μm coating thickness, the s_K values for the 0.1 μm and 2 μm coating thicknesses were 0.5% higher and 1.7% lower, respectively. These differences would have no direct clinical impact, given that S_K is determined experimentally for individual seeds. Further these changes due to coating thickness somewhat canceled with $\dot{d}_{(1,\theta_0)}$ changes when deriving Λ.

3.3.2 Λ

Table 3.5 lists Λ values using the twelve simulation conditions. In comparison to the proposed standard value (0.922 $\pm$ 0.011 cGy.h^{-1}.U^{-1}), the Λvalues of Solberg *et al*., Meigooni*et al*., and Taylor and Rogers differed by +4.3% (0.962 cGy.h^{-1}.U^{-1}), +6.2% (0.98 cGy.h^{-1}.U^{-1}), and +0.3% (0.925 cGy.h^{-1}.U^{-1}), respectively. Similarly the difference in the proposed standard value and the similarly designed model 6711 ^{125}I seed is –0.2% based on Kennedy *et al*. (0.921 cGy.h^{-1}.U^{-1}).

Table 3.5 Dose-rate constant Λ values published in the literature are compared to those obtained using the twelve simulation conditions of the current study, and the proposed standard value (simulation condition 11), along with relative values for the air-kerma strength s_K to the proposed standard value (simulation condition 11).

Investigator	Λ [cGy.h^{-1}U^{-1}]	$\frac{\Lambda}{\Lambda_{condition11}}$	$\frac{s_K}{s_{K\ condition11}}$
Solberg *et al*.	0.962	1.043	---
Meigooni *et al*.	0.98	1.062	---
Taylor and Rogers	0.925	1.003	---
Kennedy *et al*. (MC WAFAC)	0.921	0.998	---
Simulation condition 1	0.915	0.992	1.030
Simulation condition 2	0.916	0.993	1.025
Simulation condition 3	0.922	0.999	1.008
Simulation condition 4	0.886	0.960	1.025
Simulation condition 5	0.888	0.963	1.020
Simulation condition 6	0.894	0.969	1.003
Simulation condition 7	0.912	0.988	1.015
Simulation condition 8	0.951	1.031	1.004
Simulation condition 9	0.948	1.028	1.004
Simulation condition 10	0.921	0.998	0.999
Simulation condition 11	0.922	1.000	1.000
Simulation condition 12	0.896	0.971	1.009

The following observations were made upon altering the variables examined in the 12 simulation conditions

a) Increasing coating thickness linearly increased Λ. For ρ = 4.93 g/cm^3, Λ increased by 0.5% per μm increase in coating thickness.
b) Increasing coating density from ρ = 4.93 g/cm^3 to ρ = 6.003 g/cm^3 increased Λ by about 1%.
c) Values for Λ were 3.1% higher for the 02p cross-section library than the 04p cross-section library.
d) Values for Λ were 2.7% lower for the Solberg *et al*. spectrum than the NNDC-based spectrum, in agreement with the trend identified by Luxton and Jozsef,[37] in which a 3.2% diminishment of Λwould be expected for a spectrum that is 0.964 keV lower than the NNDC-based spectrum.

3.3.3 $g_L(r)$

Table 3.6 shows $g_L(r)$ results for the various simulation conditions where the proposed standard is listed as simulation condition 11. These results were compared with those published in the literature (Figure 3.2).

Table 3.6 Radial dose function, $g_L(r)$, values from the twelve different simulations. Results for simulation condition 11 are proposed as a new standard.

Coating thickness [µm]	0.1	0.5	2	0.1	0.5	2	0.5	0.5	1	1	0.5	0.5
Coating density [g/cm^3]	4.93	4.93	4.93	4.93	4.93	4.93	4.93	6.003	6.003	6.003	6.003	6.003
Cross-section library	02p	02p	02p	04p	04p	04p	04p	02p	02p	04p	04p	04p
Energy spectrum	S	S	S	S	S	S	N	N	N	N	N	S
r[cm] \Simulation Condition	1	2	3	4	5	6	7	8	9	10	11	12
0.5	1.071	1.070	1.068	1.089	1.088	1.087	1.073	1.058	1.071	1.072	1.073	1.089
1.0	1.000	1.000	0.999	1.001	1.000	1.001	1.000	1.000	1.000	1.000	0.999	1.000
1.5	0.912	0.912	0.912	0.897	0.898	0.899	0.911	0.924	0.910	0.911	0.909	0.896
2.0	0.819	0.820	0.822	0.794	0.795	0.797	0.816	0.840	0.816	0.819	0.814	0.792
2.5	0.728	0.730	0.731	0.696	0.697	0.700	0.724	0.755	0.725	0.727	0.722	0.694
3.0	0.642	0.644	0.646	0.605	0.607	0.609	0.637	0.673	0.637	0.639	0.635	0.603
3.5	0.565	0.566	0.568	0.525	0.526	0.530	0.559	0.597	0.559	0.561	0.556	0.523
4.0	0.493	0.495	0.497	0.454	0.454	0.459	0.487	0.527	0.487	0.488	0.484	0.452
4.5	0.431	0.431	0.434	0.391	0.391	0.396	0.423	0.463	0.423	0.426	0.421	0.389
5.0	0.374	0.375	0.378	0.336	0.336	0.340	0.367	0.405	0.367	0.368	0.364	0.335

5.5	0.324	0.326	0.328	0.288	0.289	0.291	0.316	0.354	0.317	0.318	0.314	0.287
6.0	0.282	0.282	0.286	0.247	0.248	0.250	0.272	0.309	0.273	0.274	0.271	0.245
6.5	0.244	0.245	0.247	0.211	0.212	0.214	0.235	0.268	0.236	0.237	0.233	0.210
7.0	0.212	0.212	0.214	0.181	0.182	0.183	0.202	0.234	0.202	0.204	0.200	0.180
7.5	0.182	0.183	0.185	0.155	0.155	0.157	0.173	0.203	0.174	0.175	0.172	0.153
8.0	0.158	0.158	0.160	0.133	0.133	0.134	0.149	0.176	0.149	0.150	0.148	0.132
8.5	0.136	0.137	0.138	0.113	0.114	0.115	0.127	0.153	0.128	0.129	0.127	0.112
9.0	0.118	0.118	0.119	0.0970	0.0973	0.0983	0.110	0.132	0.110	0.111	0.109	0.0964
9.5	0.102	0.102	0.103	0.0825	0.0830	0.0840	0.0933	0.114	0.0941	0.0947	0.0931	0.0821
10.0	0.0876	0.0876	0.0886	0.0704	0.0710	0.0714	0.0800	0.0986	0.0804	0.0805	0.0796	0.0701

n.b., For the choice of spectrum, N = NNDC-based,[24] and S = Solberg *et al*.[12]

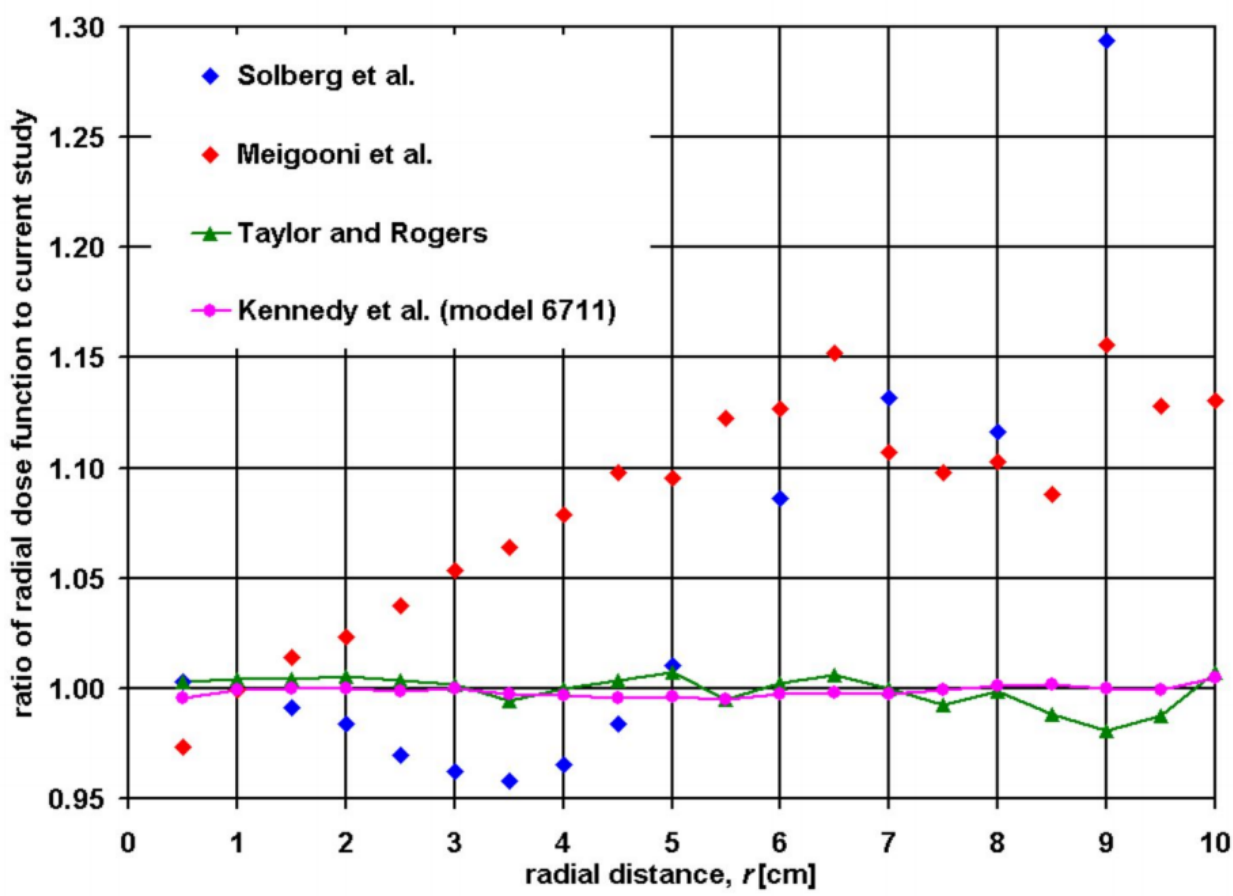

Figure 42 Ratio of $g_L(r)$ from published literature to the current study using simulation condition 11. Solid curves are used for the data points from Taylor and Rogers and for Kennedy et al. to guide the eye given their proximity to unity.

From results of the 12 different simulation conditions, changing coating thickness had a small effect on $g_L(r)$. Changes in $g_L(r)$ correlated approximately linearly with coating thickness changes and increased as r increased. For ρ = 4.93 g/cm^3, $g_L(r \geq 5)$ increased by 0.8% per μm increase in coating thickness. Changing coating density also had a small affect such that an increase in ρ from 4.93 g/cm^3 to 6.003 g/cm^3 caused $g_L(r \geq 5)$ to increase by 1%.

The 02p cross-section library consistently produced $g_L(r)$ results higher than the 04p cross-section library, with an approximately linearly relationship of +2.74%/cm with

an R^2 fit of 0.997. Thus, $g_L(10)$ using 02p was 25% larger than the value using the 04p cross-section library.

Use of the spectrum by Solberg *et al*. in comparison to the NNDC-based spectrum of simulation condition 11 influenced $g_L(r)$ in a non-linear manner by +1.5%, –2.6%, –8.2%, and –11.6% at r = 0.5, 2, 5, and 10 cm, respectively.

3.3.4 $F(r, \theta)$

Table 3.7 presents the F(r,θ) data for the model IAI I-125 seed from the MC simulation condition 11. The values increase gradually towards unity as θ approaches 90°.

Table 3.7 F(r,θ) and $\phi(r)$ values for the IsoAid model IAI I-125 ^{125}I seed determined using MC methods for simulation condition 11.

θ \ r	0.5	1.0	1.5	2.0	2.5	3.0	4.0	5.0	7.0	10.0
0	0.21	0.28	0.35	0.42	0.44	0.48	0.50	0.55	0.62	0.68
5	0.39	0.48	0.53	0.56	0.59	0.61	0.64	0.66	0.69	0.73
10	0.45	0.53	0.58	0.62	0.64	0.66	0.69	0.71	0.73	0.77
15	0.58	0.64	0.67	0.70	0.71	0.73	0.75	0.76	0.78	0.80
20	0.69	0.72	0.75	0.77	0.78	0.79	0.81	0.81	0.83	0.85
25	0.78	0.79	0.81	0.82	0.83	0.84	0.85	0.85	0.86	0.88
30	0.85	0.85	0.86	0.86	0.87	0.88	0.88	0.88	0.89	0.90
35	0.91	0.90	0.90	0.90	0.91	0.91	0.91	0.91	0.92	0.92
40	0.95	0.94	0.94	0.94	0.94	0.94	0.94	0.94	0.94	0.94
45	0.98	0.97	0.96	0.96	0.96	0.96	0.96	0.96	0.95	0.96
50	1.00	0.99	0.99	0.98	0.98	0.98	0.98	0.98	0.97	0.98
55	1.01	1.01	1.00	1.00	1.00	1.00	0.99	0.99	0.98	0.99
60	1.03	1.02	1.01	1.01	1.01	1.01	1.00	1.00	1.00	1.00
65	1.03	1.03	1.02	1.02	1.02	1.02	1.01	1.01	1.00	1.00
70	1.03	1.03	1.03	1.03	1.02	1.02	1.01	1.01	1.01	1.01
75	0.98	1.03	1.03	1.03	1.03	1.03	1.02	1.01	1.01	1.01
80	0.99	1.03	1.03	1.03	1.03	1.03	1.02	1.01	1.01	1.02
85	0.99	0.99	1.00	1.02	1.02	1.02	1.02	1.01	1.02	1.01

90	1.00	1.00	1.00	1.00	1.00	1.00	1.00	1.00	1.00	1.00
$\phi(r)$	0.98	0.97	0.96	0.97	0.97	0.97	0.96	0.96	0.96	0.97

Changes in $F(r,\theta)$ values as a function of the simulation condition variables were smaller than the observed differences between the current study (*i.e.*, simulation condition 11) and the results of Solberg *et al*. and Meigooni *et al*. The following observations were made upon altering the variables examined in the 12 simulation conditions

a) coating thickness changes of 0.4 μm, 1.5 μm, and 1.9 μm decreased $F(r,\theta)$ by > 2% at $\theta < 7°$, $\theta < 14°$, and $\theta < 17°$, respectively, using the 02p library. $F(r,\theta)$ increased by > 2% at $\theta < 8°$, $\theta < 22°$, and $\theta < 23°$, respectively,

b) changing coating density from ρ = 4.93 g/cm^3 to ρ = 6.003 g/cm^3 decreased $F(r,\theta)$ by > 2% for about $\theta < 12°$,

c) changing cross-section library from 02p to 04p increased $F(r,\theta)$ by > 2% for $\theta < 3°$, and

d) changing photon spectrum from Solberg *et al*. to the NNDC-based spectrum increased $F(r,\theta)$ by > 2% for $\theta < 24°$.

These observations were made for $0.5 \leq r \leq 10$ cm, where $F(r,\theta)$ differences generally increased as both r and θ decreased. The observed order of simulation condition variables from most to least important for influencing $F(r,\theta)$ were spectrum, coating thickness, coating density, and cross-section library.

3.4 Discussion

3.4.1 Λ

Four different photon energy spectra were used for the computations examined in the current study. Compared to the 2011 evaluation by Katakura the mean photon spectra used by Solberg *et al*., Meigooni *et al*., Taylor and Rogers as well as Kennedy *et al*. and that of the current study were all lower by 0.964 keV, 0.039 keV, 0.001 keV, and 0.003 keV respectively. From the sensitivity of Λ from sec. 3.2, only the Solberg *et al*. study would be affected by more than 0.1% due to spectral choice.

3.4.2 $g_L(r)$

From Fig. 2, differences between results of the current study (simulation condition 11) and those of Solberg *et al*. were less than 5% for $0.5 \leq r \leq 5$ cm. For larger r, disparities up to 30% were observed and mainly attributed to differences in the cross-section libraries and photon energy spectra. For a similar comparison of results for the current study and those of Meigooni *et al*., 5% agreement was observed only for $r \leq 2.5$ cm with the Meigooni *et al*. value of $g_L(2.5) = 0.750$ being 3.8% larger than those from simulation condition 11. From sec. 3.3.C, a 4.1% increase would be expected solely based on differences in cross-section libraries, which is in good agreement with the observed difference. Further, the Meigooni *et al*. value of $g_L(6.5) = 0.269$ was 15.3% larger than those from simulation condition 11. Applying the cross-section library linear correlation correction of +2.74%/cm from sec. 3.3.C, an increase of 15.1% would be expected, which was similar to the observed 15.3% difference.

Comparisons over the entire range of 0.5 $\leq r \leq$ 10 cm from simulation condition 11 to Taylor and Rogers and to Kennedy *et al*. were in agreement within 2% and 0.5%, respectively, justifying the rigor of the current study and the assumed simulation conditions.

3.4.3 $F(r,\theta)$

Upon comparing $F(r,\theta)$ values of Solberg *et al*., Meigooni *et al*., Taylor and Rogers, and Kennedy *et al*. to the proposed standard of MC simulation condition 11 as shown in Figure 3.3, substantial differences were observed at $\theta < 20°$. At F(1 cm, 10°), Meigooni *et al*. was 37% larger than the current study. At F(3 cm, 10°), results from the MC studies of Meigooni *et al*., Taylor and Rogers, and Kennedy *et al*. differed from the current study by more than 5%. This discrepancy was thought to be due to differences in the simulated end-weld thickness (see Table 3.3). These differences diminished as radial distance increased as did the proportion of radiation scatter to total dose.

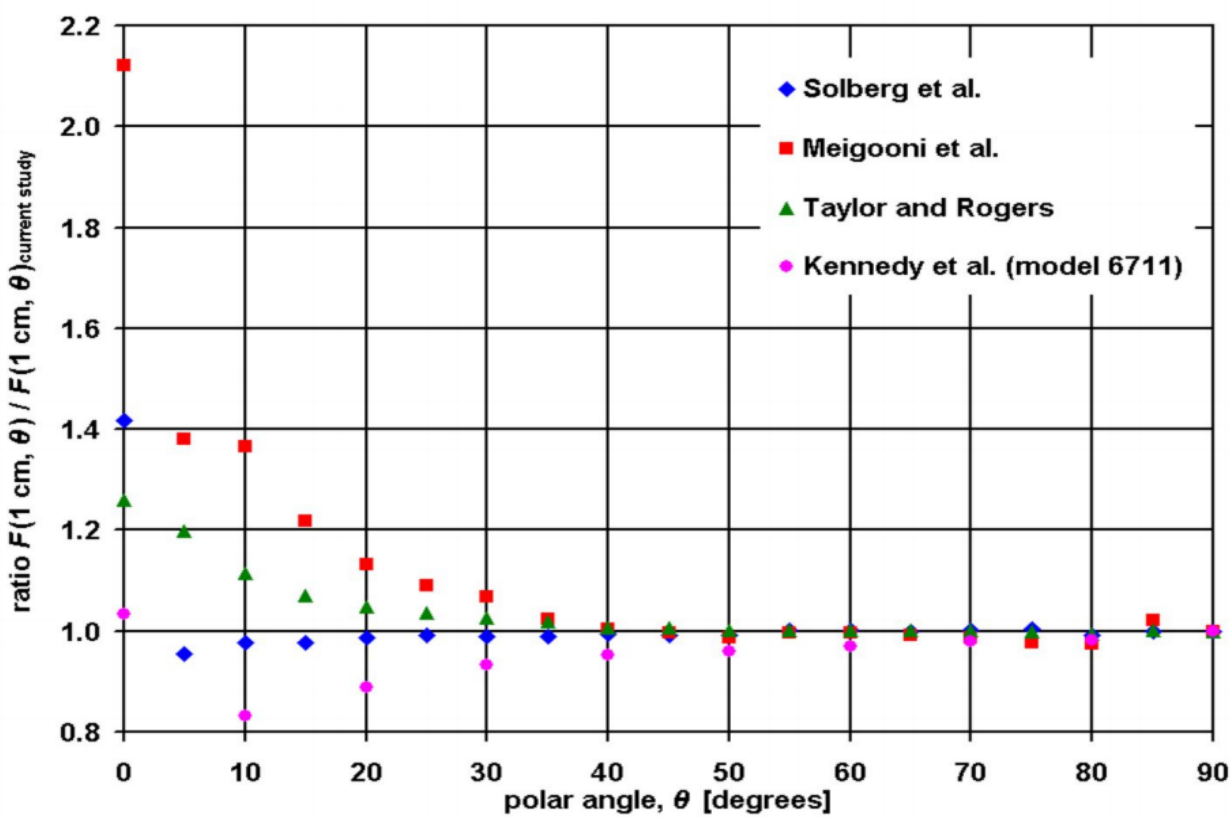

Figure 53 (a) Ratios of F(r,θ) values at 1 cm to current study (simulation condition 11). The results showed that 1-2%, 37%, 5% and 18% with Solberg et al., Meigooni et al., Taylor and Rogers, and Kennedy et al. at 10˚ respectively.

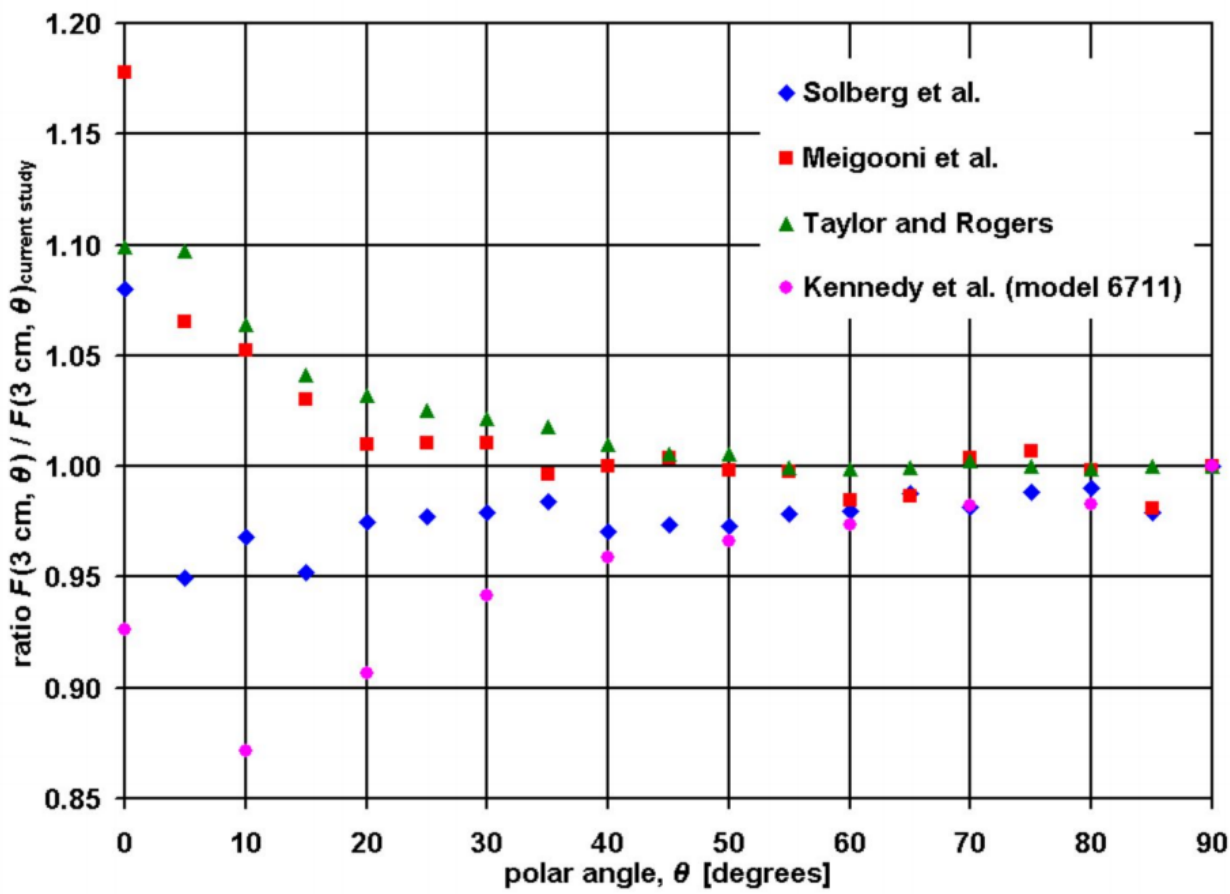

Figure 6(b) Ratios of F(r,θ) values at 3 cm to current study (simulation condition 11). The results showed that 3%, 6%, 7% and 13% with Solberg et al., Meigooni et al., Taylor and Rogers, and Kennedy et al. 10˚ respectively. The anisotropy effect was higher at smaller angle at smaller distance.

Taking from modern data for the photon interaction cross-section libraries and photon energy spectrum, the remaining simulation condition variables influencing $F(r,\theta)$ are based on the design of the model IAI-125A seed. While the design parameters in MC simulation condition 11 are thought to be most representative of the current manufacturing process, variability in the dose distribution and subsequently the resultant TG-43 dosimetry parameters such as $F(r,\theta)$ upon altering coating thickness and coating density have been gleaned. The influence of these design variables on

$F(r,\theta)$ was largest when close to the source long-axis. However, like the Λ and $g_L(r)$ results, this influence diminished to 1% when $F(r,\theta)$ was replaced with $\phi(r)$ upon using the 1D dose calculation formalism.

3.4.4 Consensus Data for Uniform Clinical Use

The AAPM consensus data for the model IAI-125A ^{125}I seed are based on results from Solberg *et al*. and Meigooni *et al*. However, examination of the simulation parameters such as varying ^{125}I coating thickness, coating mass density, photon interaction cross-section library, and photon emission spectrum indicated that significant variations in calculated dosimetry parameters may arise if modern values are not utilized. However, it is noted that simply running a new version of a transport code and using the most recent cross section libraries does not necessarily ensure improved results.[38] In the 2004 AAPM TG-43U1 report, consensus data were updated from the 1995 TG-43 report for the model 6711 ^{125}I seed and model 200 ^{103}Pd seed, but there have been no further updates of consensus data for other seeds given the recent increase of investigations on the topic of brachytherapy seed dosimetry parameters. Like the regular evaluations of nuclear data over time in other fields of physics,[24] it seems that the AAPM or other professional societies should establish a practice to regularly reevaluate consensus data given subsequent publication of results for a given brachytherapy seed.

3.5 Conclusions

Radiation transport simulations were performed using the MCNP5 code in a standardized manner for the IsoAid model IAI-125A seed for determination of the TG-43 dosimetry parameters. Several MC radiation transport codes are available for calculation of the TG-43 dosimetry parameters for brachytherapy seeds. The physics models in these codes and their related cross-section libraries have been updated and improved since the 2002 publications of Solberg *et al*. and Meigooni *et al*., as well as publication of the 2007 AAPM TG-43U1S1 report. Results using modern data indicated statistically significant differences in these dosimetry parameters in comparison to data recommended in the TG-43U1S1 report. These differences were explained by conducting a sensitivity study of results to simulation parameters such as varying ^{125}I coating thickness, coating mass density, photon interaction cross-section library, and photon emission spectrum. While the results of Solberg *et al*. and Meigooni *et al*. were used to obtain the consensus data in the TG-43U1S1 report, some simulation parameters in these two studies appear outdated. Results from Taylor and Rogers and those in the current study reflect modern assessments of the TG-43 dosimetry parameters. These results may be considered by the AAPM for reevaluating the consensus data for this seed, and for establishing a process of regular evaluations for other seeds in which the consensus data are based on methods that are no longer state-of-the-art.

CHAPTER 4 INDEPENDENT DOSIMETRIC ASSESSMENT OF THE MODEL EP917 EPISCLERAL BRACHYTHERAPY PLAQUE

4.1 Introduction

The most common cancer of the eye is uveal melanoma, and eye plaque brachytherapy is the treatment of choice for small lesions.[39,40] Brachytherapy has been used for treatment of ocular lesions since the 1930s,[41] and the Collaborative Ocular Melanoma Study (COMS) plaques have been commonly used since the 1980s for eye plaque brachytherapy.[42] The randomized, multi-institutional Phase-III COMS trial demonstrated no differences in survival between enucleation and brachytherapy for small eye lesions.[43] These COMS-style plaques are circular, 2.8 mm thick, and accommodate low-dose rate brachytherapy seeds containing ^{125}I, ^{103}Pd, or ^{131}Cs.[44]However, treatments can be problematic with 2.8 mm thick COMS plaques and for elongated tumors.[45] Therefore, other plaque designs have been proposed.[46,47]

The model EP917 brachytherapy eye plaques (IsoAid, LLC, Port Richey, FL) were initially named University of Southern California (USC #9) plaques, developed by Eye Physics, LLC (Los Alamitos, CA), and were designed to overcome the aforementioned deficiencies of the COMS plaques by collimating radiation from each brachytherapy seed with a slot machined into a gold-alloy backing. The slot designed proposed by Astrahan *et al.*[45] is depicted in Fig. 4.1a. Examination of the three EP917 plaques in our clinic indicated that that the slots were different than the design by Astrahan *et al*. and also different than the design in the Plaque Simulator (PS) treatment planning software (Eye Physics, LLC, Los Alamitos, CA). To resolve these discrepancies, an investigation was performed to accurately measure the eye plaque slots and overall design, and to determine the dosimetric influence of eye plaque design variations using Monte Carlo (MC) methods for radiation transport simulations. This type

of study, to independently assess the reported design of the Eye Physics plaques, has not been performed previously to our knowledge, and demonstrates the need for a robust acceptance testing procedure.

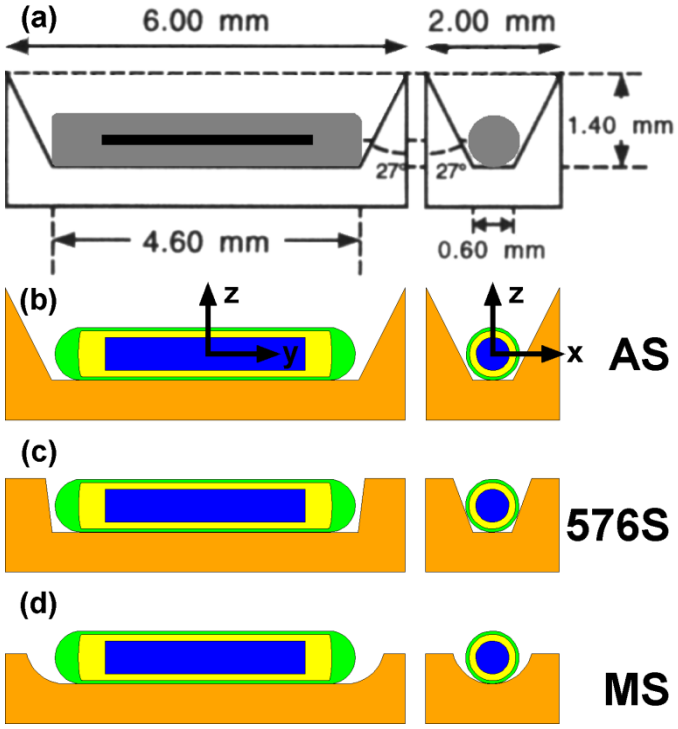

Figure 4.1 Various slot designs are possible with eye plaque brachytherapy. (a) the slot design proposed by Astrahan et al. as adapted from their Fig. 2, (b) simulated geometry of the Astrahan et al. slot (AS) with slot length and width of 6.00 mm and 2.00 mm, respectively, with a slot depth of 1.40 mm, (c) simulated geometry of the Plaque Simulator version 5.7.6 slot (576S) with slot length and width of 4.79 mm and 1.18 mm, respectively, with a slot depth of 0.81 mm, and (d) simulated geometry of the measured slot (MS) with length, width, and depth of 5.40 mm, 1.20 mm, and 0.46 mm. respectively. The left and right sides show longitudinal and transverse planes, respectively, through the slots and seeds. All Monte Carlo simulations were for the model IAI-125A ^{125}I seed.

Marwaha *et al.*[48] showed that the dose to macula, optic disc, and opposite retina structures was reduced by 13.2%, 5.4%, and 0.6% respectively, using the model EP917 plaque in comparison to COMS plaques. However, the slot dimension including the

depth of such plaques was not mentioned. Zimmermann *et al*.[49] compared doses calculated using PS v.5.7.4 and MC methods for the model EP917 plaque loaded with the model IAI-125I ^{125}I seed (IsoAid, LLC, Port Richey, FL) loading only the central slot, i.e., slot #1 in v.5.7.6 in PS. PS doses differed from the MC results by 32.4% and 12.5% at 1 mm and 2 mm from scleral surface, but matched within 5% for depths ranging from 3 mm to 12 mm. However, this abstract did not examine a fully-loaded plaque or provide dimensional information on the planned or simulated slots. Consequently, we hypothesized that plaque design differences would substantially influence dose distributions for episcleral brachytherapy.

4.2 Methods and Materials

4.2.1 Monte Carlo methods

Version 1.40 of the MCNP5 MC radiation transport code[50] was used for simulation of 2D and 3D dose distributions. The collision kerma was approximated as absorbed dose for low energy photons, and electron transport was ignored. The default MCNP v.1.40 photon cross-section library (MCPLIB04) was used for all simulations, and the *F4 track length estimator was used with tally modifiers based on mass-energy absorption coefficients from the National Institute of Standards and Technology.[51] The most recent ^{125}I photon energy spectrum from the National Nuclear Data Center[52]was used in these simulations, including the 3.77 keV photon, which may contribute to dose within 1 mm of the source in water or tissue. A total of 10^{10} photon histories were simulated for each slot and plaque design to minimize the statistical uncertainties. In general, the MC simulation methods performed by Rivard *et al*. were followed.[53]However, the medium surrounding the single-slot geometries and the eye plaques adjacent to the ocular globe were surrounded with a 10 cm diameter sphere of liquid water (0.998 g/cm^3). All materials (other than the ^{125}I seeds and the gold alloy) were assumed to be composed of water, and all reported dose values are to water in water.

4.2.2 Slot Designs

To glean insight into the potential reasons for dosimetric differences in plaques having differing slot designs, the geometry of a single slot was considered. The primary comparison was between the manufacturer-reported slot dimensions and the measured

slot dimensions. Astrahan *et al*. published a slot length, width, and depth values of 6.00, 2.00 mm, and 1.40 mm, respectively (Fig. 4.1a).[45] However, values for these dimensions included in the most recent version of the PS software (version 5.7.6) available to us as of this writing were smaller, *i.e.*, 4.79, 1.18, and 0.81 mm, respectively. Consequently, slot dimensions values from the PS software were taken as the manufacturer-reported slot dimensions for simulations (Fig. 4.1b) and are referred to as 576S.

Measurements were performed to independently evaluate this and resolve the dimensional differences between this publication and the values provided in the PS software. Using a ruler calipers, and photomicroscopy,[54] the slot was determined to have a circular cross section and to have hemispherical ends (Fig. 4.1c) instead of the isosceles trapezoidal cross-section described by Astrahan *et al*. or utilized in the PS software. This fits with our understanding of the manufacturing process for our plaques, in which a rounded bit was used with a dental tool for slot fabrication. Fig.1B in Marwaha *et al*.[48] and in Berry *et al*.[55] also depict slots having rounded ends. For three model EP917 plaques, the measured lengths and widths for the slots were 5.4 mm and 1.2 mm, respectively, with a variation of about 0.1 mm (k=1) in both dimensions. The measured depth (at the midpoint of the seed) for 51 slots (three plaques) ranged from 0.16 mm to 0.73 mm, with an average depth of 0.46±0.16 mm (k=1). Depth measurement precision was estimated as 0.04 mm (k=1). There was no observed correlation in slot depth as a function of distance from the plaque central axis (CAX) or other physical aspects. Measurements at another institution having the same plaque model were in agreement with the slot depths determined in the current study.[56]

Due to the plaque curvature to conform to the eye, slot depths increased towards the slot ends since the slot bottoms were not curved to accommodate the seeds (Fig. 2a). However, for the study of single-slot dosimetry, a single value was chosen for characterizing the slot depth. This measured slot design (referred to as MS) was compared through simulations of the slot geometries by Astrahan *et al*. (AS) and the 576S design.

Secondary comparisons of variants of the measured slot design evaluated the sensitivity of the dose distribution to design variations and assumptions inherent to the simulations. These variations include plaque mass density ρ and plaque composition; slot length, width, and depth; seed positioning; and Ag-marker rod positioning. The nomenclature of nMS represents narrow slots (5.00, 0.80, and 0.46 mm long, wide, and deep, respectively) and dMS represents narrow and deep slots (5.00, 0.80, and 0.97 mm long, wide, and deep, respectively). These nMS and dMS slots were theoretically designed and simulated to examine the sensitivity of dose distribution to the slot design.

Quantitative tolerances for applicator dimensions were not provided in the AAPM TG-40 report on radiation oncology quality assurance,[57] the AAPM TG-56 report establishing a brachytherapy code of practice for medical physics,[58] or the ESTRO Booklet 8 on European brachytherapy quality assurance standards.[59]However, the AAPM TG-40 report (Table XI) recommended that brachytherapy applicators be inspected upon initial use and yearly, and that brachytherapy dose should be delivered within 5% limits. Therefore, a dose change of 5% was used to categorize a change in slot design as being important.

The plaque manufacturer indicates that the plaque is composed of 18K gold. However, the ρ and composition of 18K gold is not standardized.[60,61,62,] A value of ρ=15.58 g/cm^3 has been cited,[60] but this is dependent on alloy composition. Characteristic x ray production is dependent on the plaque composition, and low-energy photons emitted from low dose-rate brachytherapy seeds such as ^{125}I, ^{103}Pd, and ^{131}Cs induce x ray production in the elements comprising the alloy. These characteristic x rays emanate from Au, Ag, and Cu with energies of 11-13 keV (L-edge), 22-25 keV (K-edge), and 8-9 keV (K-edge),[63,64] respectively, and enhance the dose near the seed due to fluorescent photons and the photoelectric effect. To evaluate the dosimetric influence of altering the gold alloy ρ and composition, simulations of the MS slot design were performed for ρ=15.58 g/cm^3 and an extreme case of ρ=19.3 g/cm^3, and for proportions by mass of Au:Ag:Cu from 75%15%10% and 75%2.75%22.25%, respectively.[61,62]These compositions are referred to as Ag=15% and Ag=2.755%, respectively. Dose ratios of these combinations were used to evaluate the importance of each material property, i.e., ρ and composition, for the MS slot design. An additional simulation was performed for the Astrahan *et al*. slot design to evaluate the dosimetric importance of changing the 18K gold alloy mass density and composition from ρ=15.58 g/cm^3 to ρ=19.3 g/cm^3 and Ag=15% to Ag=2.755%, referred to as $_{alloy}$AS in the current study.

The model IAI-125A ^{125}I seed was positioned in every slot design evaluated.[65] To determine the sensitivity of dose to position of this seed within a slot, the entire seed was offset laterally within the slot by 0.0994 mm, vertically out of the slot by 0.0994 mm, and/or longitudinally along the slot by 0.3495 mm. These shifts (Table 4.1) corresponded approximately to the maximum possible shifts without capsule collision

with the slot or penetration into the ocular globe. Further, the Ag-marker rod within the ^{125}I seed capsule was also shifted (Table 4.1) maximally to account for dynamic internal components.[66] The rod was offset laterally within the capsule by 0.0994 mm, vertically towards the ocular globe by 0.0994 mm, and/or longitudinally towards the capsule endweld by 0.3495 mm. These rod shifts were the maximum possible within the capsule. Subsequently, the entire seed was shifted by the same amount as the rod. This was done so that dosimetric differences due to shifting of the Ag rod or the surrounding Ti capsule could be separately identified.

For all slots designs evaluated, dose was estimated on three orthogonal planes. The in-plane resolution was $(0.01\ cm)^2$ with an overall extent of $(2.51\ cm)^2$ for a 251×251 array on the xz, yz, and xy planes (Fig. 4.1b). The planar thickness was chosen as 0.01, 0.05, and 0.05 cm, respectively, to minimize in-plane dose gradients. Dose along the slot CAX at 1, 2, 5, and 10 mm from the origin along the z axis was also evaluated. The coordinate system origin for the single-slot study was at the center of the ^{125}I seed.

Table 4.1 It is possible to shift the seed position within the slot, and the Ag rod within the IAI-125A ^{125}I seed to move within the Ti capsule. Monte Carlo simulations were performed with shifts based on the measured dimensions of the reference slot design (MS). Variants of seed offsets and rod offsets were examined to evaluate their dosimetric influence. Values for all dimensions are in millimeters.

Offset	Seed xz	Seed y	Seed z	Seed yz	Rod x	Rod y	Rod z	Rod yz
Seed x	0.0994	0	0	0	0	0	0	0
Seed y	0	0.3495	0	0.3495	0	0	0	0
Seed z	0.0994	0	0.0994	0.0994	0	0	0	0
Rod x	0	0	0	0	0.0994	0	0	0
Rod y	0	0	0	0	0	0.3495	0	0.3495
Rod z	0	0	0	0	0	0	0.0994	0.0994

4.2.3 Plaque designs

From the dosimetric study of the slots, five slot designs were included for evaluation of the model EP917 plaque having 17 slots in total. This included the measured slot (MP) and variants to explore dosimetric sensitivity to slot design variations (Table 4.2) with the last letter “P” indicating plaques where “S” was used in Sec. 2.B for single slot simulation. While the slot shape from the PS software was accurately simulated for the single-slot study, the exact slot shape used in PS to perform treatment planning for the model EP917 plaque could not be simulated because of overlap at the slot corners. Consequently, slot dimensions from the PS software were approximated (576P) and are indicated in (Table 4.2). A narrow version of the reference measured plaque, *i.e*., nMP, was also examined. The original slot design of Astrahan *et al*. was not included in the dosimetric evaluation of plaques because the slots would substantially overlap given the measured slot positions. Also, in

contrast to the single-slot simulations where the measured slot depth (at the midpoint of the slot length) was consistent over the entire length of the slot due to the rectangular geometry, the slot depth varied for simulations with the curved plaques and the slot design from Astrahan *et al*. could not physically fit within the 1.0 mm thick plaque. Therefore, the dosimetric influence of changing the slot length, width, and depth was examined in the dMP plaque design (Table 4.2) where the seed position was kept at the bottom of the slot and subsequently moved 0.51 mm away from the ocular globe due to the deeper slot depth.

Table 4.2 Several plaque designs were examined using Monte Carlo methods. The slot dimensions are given in millimeters.

Plaque	Description	Length	Width	Depth
576P	Plaque Simulator v.5.7.6 approximation	4.50	1.06	0.60
MP	measured slot for standard plaque	5.40	1.20	0.46
sMP	shift rod 0.0994 mm toward globe	5.40	1.20	0.46
nMP	narrow slot length and width	5.00	0.80	0.46
dMP	narrow slot length and width, deep slot, and 0.51 mm seed shift away from globe	5.00	0.80	0.97

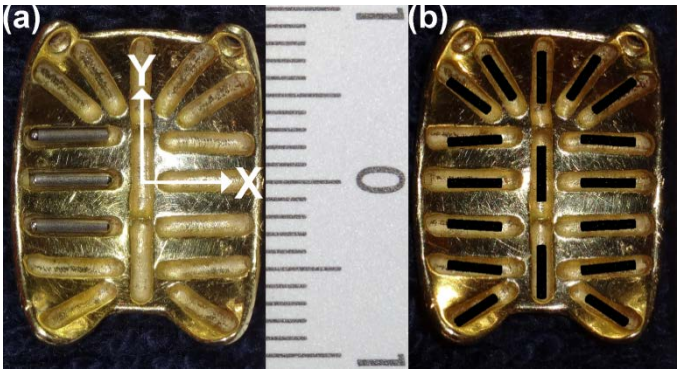

Figure 4.2 Slot positions for the model EP917 eye plaque were based on measurements using photomicroscopy. The plaque (a) is loaded with three dummy ^{125}I seeds (model IAI-125A), and the reference Monte Carlo simulation model showing simulated positions of the ^{125}I-laden cylindrical Ag rods within the Ti capsules (b). The Z-axis direction points out of the page. The ruler indicates units in centimeters with increments in millimeters.

In versions of the PS software used at the start of this investigation (v.5.3.6 and v.5.3.7), 13 of the 17 slots overlapped and were physically implausible. As the plaques did not exhibit the overlap as indicated by the PS software and the slots were not symmetric about the YZ plane (Fig. 4.2a), measurements were performed to independently obtain the coordinates and orientations for the 17 slots. High-resolution images (3672×4866 pixels) of the model EP917 plaques were taken with a digital camera (model DSC-HX20V, Sony Corp., Tokyo, Japan). The camera settings and position (i.e., 20 cm) relative to the plaque were such that image divergence was minimal.

Camera image accuracy was verified by examining a fixed grid and quantifying any image distortion. The barrel effect due to von Seidel aberrations was measured over the central region of the image where the plaque was located.[67,68] Image distortion

was about 0.2% at the corners of the plaque image, which corresponded to an error of about 1 pixel (about 0.012 mm). Thus, the plaque images were considered to be accurate and the assignment of spatial position in terms of pixels was valid. This finding was further validated by examining the ruler (positioned beyond the plaque) where differences between the millimeter scales across the field-of-view (7 mm lateral and ±10 mm longitudinally) were also no more than 1 pixel. Consequently, slot position measured on the image was used for the simulated slot position in the plaque (Fig. 4.2b). Orientation of the slots out of the image plane was accounted for using trigonometric calculations based on the plaque curvature about the ocular globe. The slot coordinates from the PS software (version 5.7.6) and the measured results are given in Table 4.3. The average distance between PS and measured slot centers was 0.07 cm (range 0.02-0.10 cm). The main difference was our assignment of the Y axis along slots #7 and #14 (Table 4.3), whereas PS v.5.7.6 placed slot #1 at Y=0. When accounting for this 0.07 cm offset in the Y direction, the average distance was then 0.04 cm (range 0.01-0.06 cm).

Table 4.3 Slot center coordinates from the Plaque Simulator software (version 5.7.6) and measured using photomicroscopy for the model EP917 plaque. The coordinate system is indicated in Fig. 4.2a and Fig. 4.3. Values for all dimensions are in centimeters.

	PS v576 coordinates			Measured coordinates		
Slot	X	Y	Z	X	Y	Z
1	0.000	0.000	-0.160	0.000	0.050	-0.141
2	0.000	0.494	-0.062	0.000	0.578	-0.004
3	0.009	-0.494	-0.062	0.000	-0.487	-0.045
4	-0.239	0.513	-0.029	-0.231	0.576	0.020
5	-0.407	0.421	-0.019	-0.399	0.476	0.020
6	-0.399	0.161	-0.086	-0.367	0.231	-0.066
7	-0.395	-0.055	-0.097	-0.367	0.000	-0.088
8	-0.386	-0.324	-0.057	-0.367	-0.231	-0.066
9	-0.342	-0.547	0.013	-0.367	-0.463	0.003
10	-0.331	-0.779	0.156	-0.359	-0.696	0.128
11	0.371	-0.761	0.156	0.359	-0.696	0.128
12	0.361	-0.535	0.013	0.367	-0.463	0.003
13	0.370	-0.311	-0.066	0.367	-0.231	-0.066
14	0.373	-0.059	-0.104	0.367	0.000	-0.088
15	0.364	0.162	-0.097	0.367	0.231	-0.066
16	0.414	0.414	-0.019	0.399	0.476	0.020
17	0.239	0.513	-0.029	0.231	0.576	0.020

The coordinate system origin for the plaque simulations differed from the single-slot study. The z=0 position for the slot was centered in the seed and the Z=0 position for the plaques was positioned along the plaque CAX at the inner sclera (Fig. 3). The plaque was simulated as being symmetric about the YZ plane at X=0. This assumption

was considered reasonable based on the observed manufacturing tolerances when comparing the three model EP917 plaques. Except for the dMP design where seeds were 0.51 mm from the outer sclera, the seeds within the plaque were simulated as being in contact with an eye. The plaque and ocular globe were centered in a 5 cm radius water sphere to provide photon scattering conditions to approximate an infinitely large phantom. A tumor was simulated (Fig. 4.3) with a basal diameter of 11 mm and an apical height of 5 mm,[69] and aligned with its CAX oriented along the Z axis with the tumor apex positioned at Z=0.5 cm. To simulate human anatomy as a means of modeling dose-associated toxicity, the inner sclera (to approximate retinal dose) was defined at an ocular radius of 1.13 cm, and the outer sclera was defined at an ocular radius of 1.23 cm.

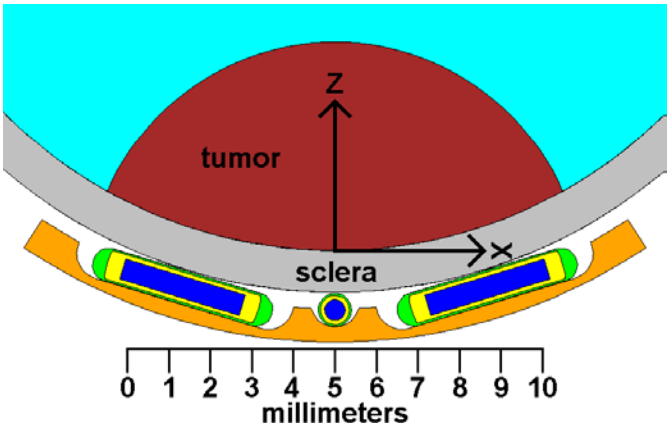

Figure 4.3 Monte Carlo dose calculation environment depicting a simulated model EP917 brachytherapy eye plaque (MP) loaded with model IAI-125A ^{125}I seeds centrally positioned within each slot. As would be performed for a clinical procedure, the simulated plaque is in contact with an eye having a 1 mm thick sclera. Also shown is a simulated tumor with a basal diameter of 11 mm and an apical height of 5 mm. The coordinate system origin is located on the plaque CAX at the inner sclera (Z=0), with the Y axis pointing out of the page.

As was performed for the slot design assessment, dose was estimated on three orthogonal planes for the plaque study. Further, dose volume histograms (DVHs) were created for the tumor, inner sclera, and outer sclera. These volumes were radially segmented about the Z axis with 0.01 cm resolution. The tumor volume was further subdivided along the Z axis with 0.02 cm resolution, for a total of 536 volume elements. Dose in the scleral regions was obtained for $Z \leq 0.5$ cm with 0.1 μm thick voxels to minimize dose volume averaging. There were 94 and 106 volume elements for the inner sclera and outer sclera, respectively. These volume elements were created where the tumor was introduced and the EP917 plaque would be positioned. The DVH results were further analyzed through consideration of the high dose region using D_{10}, the dose delivered to at least 10% of the volume for the tumor, inner sclera, and outer sclera.

The prescription at our institution for a 96 h implant has been a dose of 85 Gy to the tumor apex. Using the PS software with the revised dosimetry data for the model IAI-125A ^{125}I seed,[65] this required 3.279 U per seed. To provide direct comparisons between the PS software results and the MC results, raw values for the simulated dose were corrected according to the methods of Melhus and Rivard.[70] For the model IAI-125I ^{125}I seed, the conversion factor from native MCNP output (i.e., MeV/g/s.p.) to Gy was determined to be 222,452±222 (k=1). Consequently, the MC results were reported in terms of Gy for the same prescriptive criterion, 3.279 U/seed for a 96 h implant. Due to the substantial slot-design differences between the dMP and MP plaques, doses from the dMP plaque were normalized to match the MP dose at 0.5 cm on the CAX for comparison with the other simulated plaques. The normalized dMP plaque results are referred to as dMP'.

4.3. Results

4.3.1 Slot Design

4.3.1.1. Mass Density and Plaque Composition

Using the notation defined in Sec. 2.A for gold-alloy ρ and composition, the dose ratio for the standard MS slot design with $D_{\rho=19.3}/D_{\rho=15.58}$ was 0.999 at 1 mm from the source, equilibrating to about 0.998 beyond 3 mm. The dose ratio for the standard MS slot design with $D_{Ag=0.15}/D_{Ag=0.02755}$ was 0.993 at 1 mm from the source, equilibrating to about 0.985 at larger distances. Statistical uncertainties (k=1) were <0.1%. When both mass density and gold-alloy composition were altered for the MS slot design, there were no statistically-significant differences with the conditions where only composition was altered. The dosimetric influence of changing gold-alloy ρ or composition was largest along the CAX of the slot aperture. At locations outside the slot aperture where radiation scatter dominated, changing gold-alloy ρ or composition produced even smaller effects.

The dose ratio ($_{alloy}$AS/AS) for the slot design by Astrahan *et al*. was 0.985 at 1 mm from the source, equilibrating to about 0.976 beyond 3 mm. Given the slot design by Astrahan *et al*. was deeper than the MS slot design (i.e., 1.4 mm versus 0.5 mm), more photons interacted with the gold alloy and consequently the influence of gold-alloy ρ and composition was more important for the slot design by Astrahan *et al*. However, most of this effect is thought to be due to the gold-alloy composition as simulations of only changing ρ for the MS slot design indicated minimal influence. Regardless, changing gold-alloy ρ or composition for the MS or AS slot designs did not exceed the 5% threshold for importance.

4.3.1.2. Slot Dimensions

For the MS slot design, Table 4.4 presents the influence of altering slot length, width, and depth on CAX dose at 1, 2, 5, and 10 mm, respectively. Statistical uncertainties (k=1) were <0.1%. While statistically significant variations in dose were observed, none of these changes surpassed the 5% threshold considered to be important for slot design variations.

Table 4.4 The influence of slot length, width, and depth on dose variation along the CAX at source distances of 1, 2, 5, and 10 mm for the measured plaque (MP) respectively. In all cases, the dose perturbation due to these variations was less than 2.0%.

CAX	Δ slot length (mm)		Δ slot width (mm)				Δ slot depth (mm)			
(mm)	–0.1	+0.1	–0.1	+0.1	+0.2	+0.3	–0.2	–0.1	+0.1	+0.2
1	1.000	1.000	1.006	1.013	1.015	1.016	0.991	0.995	1.015	1.013
2	1.001	1.000	1.004	1.013	1.015	1.017	0.997	0.999	1.008	0.999
5	0.994	1.000	1.004	1.012	1.015	1.016	1.008	1.005	1.002	0.987
10	1.014	1.001	1.006	1.012	1.016	1.018	1.016	1.010	1.000	0.983

4.3.1.3 Shifts of Seeds and Rods

The results in Table 4.5 had statistical uncertainties (k=1) <0.1%, and indicate that CAX doses for $1 \leq y \leq 10$ mm were within 5% of the MS CAX dose results. These small differences were thought to be due to scatter conditions because of different slot collimations. However, the CAX doses for the sMS slot design with the ^{125}I-laden Ag rod shifted 0.0994 mm away from the slot (z direction) exhibited higher doses (14.2% at 1 mm and 8.8% at 2 mm) than the MS design. These dose differences were thought to be due to geometric effects, e.g., inverse-square, by positioning the radiation source closer to the CAX point of interest. Increases of 16.4% at 1 mm and 9.3% at 2 mm would have been expected due to geometry alone.

Table 4.5 The influence of shifting the seed or rod on dose variation along the CAX at source distances 1, 2, 5, and 10 mm respectively. Shifts in the x, y, and z directions correspond to the transverse direction along the source midplane bisector, along the source long axis, and outside the slot towards the ocular globe for MS slot respectively.

CAX	Seed shift			Rod shift		
(mm)	x=0.0994 mm	y=0.3495 mm	z=0.0994 mm	x=0.0994 mm	y=0.3495 mm	z=0.0994 mm
1	0.992	0.984	1.154	0.964	0.983	1.142
2	0.994	0.984	1.094	0.966	0.984	1.088
5	0.998	0.995	1.048	0.969	0.994	1.043
10	0.999	0.996	1.031	0.966	0.994	1.027

4.3.1.4. CAX Slot Dose Ratios

For the AS, 576S, nMS, and dMS slot designs, statistical uncertainties (k=1) were <0.1%. The results in Table 4.6 indicate that CAX doses for $1 \leq z \leq 10$ mm were within 5% of the MS CAX dose results. The ratio of CAX doses of sMS and MS was the same as reported in Table 4.5. Differences in CAX dose ratios for the other slot designs were thought to be due to differing scatter conditions along the CAX because of different slot collimations. All statistical uncertainties (k=1) for Table 4.6 were <0.1%.

Table 4.6 The influence of altering the slot dimensions on the ratio of CAX doses of different slot designs to the measured slot design.

CAX (mm)	AS / MS	576S / MS	sMS / MS	nMS / MS	dMS / MS
1	1.047	1.009	1.142	0.991	0.998
2	1.035	0.994	1.088	0.990	0.985
5	0.988	0.977	1.043	0.989	0.973
10	0.966	0.969	1.027	0.990	0.967

4.3.2 Plaque Design

4.3.2.1. CAX Dose Comparison

For the plaque designs described in Table II, the results in Table VII indicate that the CAX dose ratios to the MP plaque were within 5% except for the sMP plaque having the rods shifted 0.0994 mm towards the ocular globe and for the dMP plaque having the seeds shifted 0.51 mm away from the ocular globe. The large dose changes for these two plaques were mainly thought to be due to changes in geometric effects by positioning the radiation source closer and farther from the CAX point of interest, respectively. It is evident that changing the slot length, width, and depth (i.e., 576P and nMP) did not make large changes to the CAX dose ratio. Also included for comparison is the CAX dose ratio of the PS software to the MP results. The planned dose of 85 Gy to the tumor apex (Z=0.5 cm) using PS appears to deliver 88 Gy. The statistical uncertainties (k=1) were <0.1% in contact with the globe, <0.2% at the tumor apex (Z=5mm), and <0.7% at the opposite position in the eye from the plaque.

Table 4.7 The influence of altering the slot design for the model EP917 eye plaque. CAX dose ratios for are taken in comparison to the plaque using the reference measured plaque design (MP). The 576P plaque has slots approximating values used within the Plaque Simulator software and the PS v.5.7.6 results are taken from the treatment planning system. The sMP plaque has the ^{125}I-laden Ag rods shifted 0.0994 mm towards from the ocular globe; the nMP plaque has narrow slot lengths and widths; and the dMP plaque has narrow slot lengths and widths with deeper slots and the seeds shifted 0.51 mm shift away from ocular globe. Also included are the dMP' results, being the dMP results normalized (+25%) to match the MP dose at the tumor apex (Z=0.5 cm).

CAX (mm)	576P / MP	PS v.5.7.6 / MP	sMP / MP	nMP / MP	dMP / MP	dMP' / MP
–1	0.951	0.928	1.343	0.983	0.306	0.380
0	0.947	0.921	1.050	0.972	0.581	0.722
1	0.970	0.965	1.032	0.985	0.665	0.826
2	0.979	0.966	1.030	0.988	0.718	0.891
5	0.984	0.967	1.028	0.989	0.804	1.000
10	0.974	0.996	1.022	0.987	0.830	1.034
15	0.972	0.996	1.017	0.988	0.833	1.035
20	0.979	0.998	1.015	0.988	0.845	1.047
22.6	0.990	0.997	1.020	0.986	0.842	1.049

4.3.2.2 2D Dose Comparison

Dose distributions for the examined plaques did not vary substantially, except for the dMP plaque design and the normalized dMP' design. Fig. 4.4 depicts dose

distributions on the XZ plane for some of these plaque designs, and also includes dose distribution results adapted from the PS software for a side-by-side comparison with the 576P simulation results. The tumor volumes between the simulated environment (0.262 cm^3) and the PS software (0.29 cm^3) were similar, as also indicated graphically by the tumor outlines in Fig. 4.4c and Fig. 4.4d, respectively. Based on this figure and Table 4.7, the CAX doses between the simulated are quite similar (within 3% at all distances examined), and substantially differ only at locations far from the CAX. Ratios of dose distributions on the XZ plane for the 576P and dMP' plaque designs relative to the MP design are shown in Fig. 4.4e and Fig. 4.4f, respectively. From these results in comparison to the MP plaque design, it is evident that the dMP' design minimizes the dose gradient across the tumor while diminishing dose laterally with only small increases in dose at the largest distances along the CAX (i.e., +5% for $Z \geq 2.0$ cm).

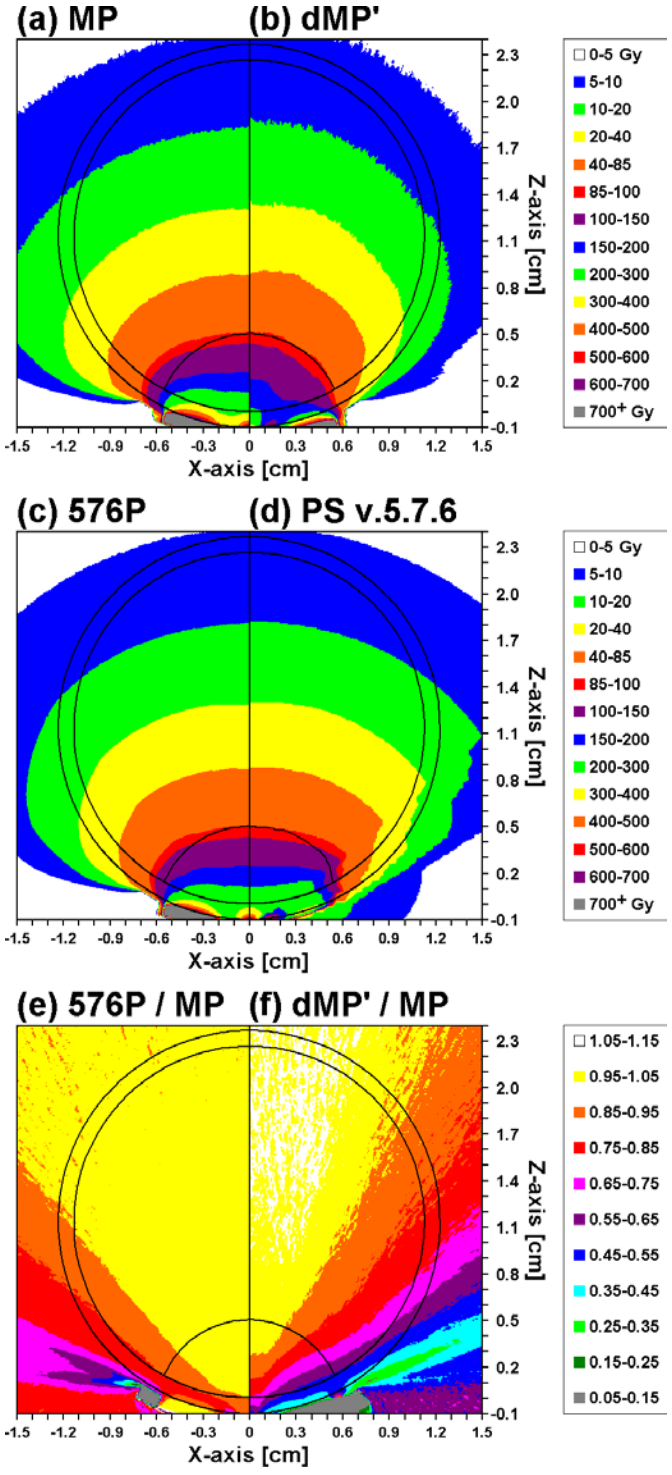

Figure 4.4 The ocular globe periphery (2.46 cm diameter) and inner surface are indicated by the black circles with the tumor border similarly indicated. The tumor shape from the Plaque Simulator software is included for comparison. Dose distributions on the XZ plane for (a) the measured plaque design (MP), (b) the normalized results for the

deep and narrow plaque design (dMP'), (c) the simulated plaque used in the Plaque Simulator software (576P), and (d) results from the Plaque Simulator treatment planning software (PS v.5.7.6) to deliver 85 Gy to the tumor apex (Z=0.5 cm) in 96 h. Comparing the MP and dMP' dose distributions, it is evident that 85 Gy isodose line is more conformal for the dMP' plaque design than the MP design. Also apparent is the decreased dose gradient within the tumor and the increased dose conformity laterally outside the eye, with slight dose increase along the plaque central axis, i.e., Z-axis. Comparing the 576P and PS v.5.7.6 dose distributions, the central axis depth doses are similar, but the PS v.5.7.6 results exhibit substantial dose lateral to the plaque (i.e., X>0.6cm and Z=0cm). The dose ratio (e) of the 576P plaque design to the MP measured plaque design (576P/MP) is within 5% of unity throughout much of the ocular geometry, decreasing substantially towards the plaque rim (i.e., X=0.7cm and Z=0.1cm). The dose ratio (f) of the dMP' plaque design to the MP measured plaque design (dMP'/MP) shows greater variability, which may be interpreted through comparing (a) and (b).

4.3.2.3 DVHs for the Plaques

The DVHs for the tumor, inner sclera, and outer sclera are depicted in Fig. 4.5, and demonstrated the same trend as the CAX dose ratios in Table 4.7. When considering the tumor DVH, it appears that there were no substantial differences among the examined plaque designs except for the dMP having deep and narrow slots. However, differences between the plaques were more pronounced for the inner and outer sclera, albeit following the same trend as exhibited for the tumor.

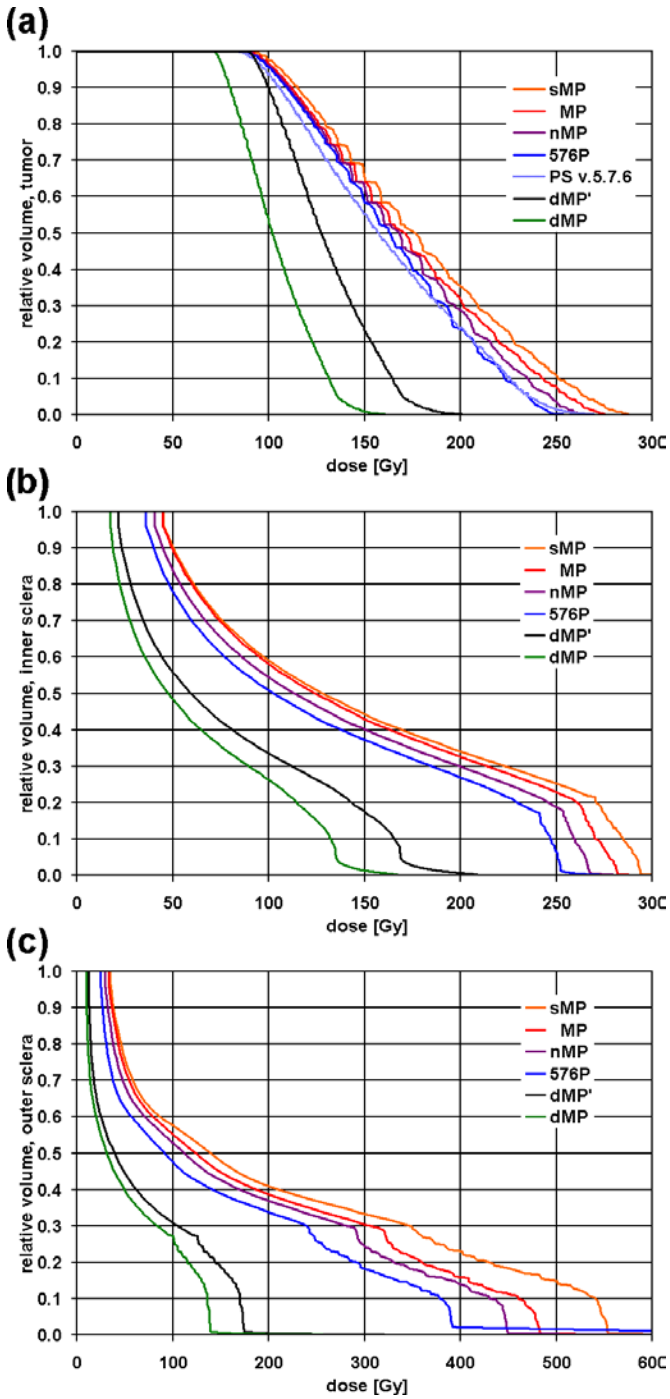

Figure 4.5 DVHs for the (a) tumor, (b) inner sclera, and (c) outer sclera for the model EP917 eye plaque loaded with model IAI-125A ^{125}I seeds. Consistently, the sMP plaque having the ^{125}I-laden Ag rods shifted 0.0994 mm towards from the ocular globe had the largest values for all three volumes, with the reference measured plaque (MP), narrow plaque (nMP), simulated Plaque Simulator plaque design (576P), results from the Plaque Simulator treatment planning software (PS v.5.7.6), and the deep and narrow

plaque (dMP) following consecutively. Also included are the dMP' results, being the dMP results normalized (+25%) to match the MP dose at the tumor apex (Z=0.5 cm).

Ratios of tumor D_{10} values for the examined plaque designs to the MP design are given in Table 4.8. To understand these ratios in absolute dose, the MP D_{10} values for the tumor, inner sclera, and outer sclera were 242.3, 270.4, and 460.0 Gy, respectively. For example, tumor D_{10} for the dMP design was 130.3 Gy. In comparison to the simulated PS plaque (i.e., 576P), the D_{10} dose ratio determined using the PS software (i.e., PS v.5.7.6) was 2% higher. The ratio of D_{10} for the outer sclera to the inner sclera was 1.70 on average (i.e., 1.70 for MP, 1.53 for 576P, 1.89 for sMP, and 1.66 for nMP) except for the dMP design, which had a ratio of only 1.027. Thus, the dMP design appeared to provide substantial reduction in the high-dose gradient over the ocular globe.

Table 4.8 The D_{10} ratios for various plaque designs to the MP plaque design for the tumor, inner sclera, and outer sclera. Ratios to the measured plaque design (MP) are taken for the simulated Plaque Simulator plaque design (576P), results from the Plaque Simulator treatment planning software (PS v.5.7.6), a simulated plaque having the ^{125}I-laden Ag rods shifted 0.0994 mm towards from the ocular globe (sMP), a simulated plaque having narrow slot lengths and widths (nMP), and a simulated plaque having narrow slot lengths and widths with deeper slots and the seeds shifted 0.51 mm shift away from ocular globe (dMP). The dMP' plaque results are the dMP results normalized (+25%) to match the MP dose at the tumor apex (Z=0.5 cm). The tumor D_{10} ratio (i.e., 0.931) for the Plaque Simulator software results to the reference measured plaque design is provided (PS v.5.7.6 / MP). However, it was not feasible to enter the scleral geometries simulated using Monte Carlo methods into the Plaque Simulator software, and thus no ratios are provided.

Ratio	Tumor	Inner sclera	Outer sclera
576P / MP	0.912	0.905	0.814
PS v.5.7.6 / MP	0.931	---	---
sMP / MP	1.026	1.045	1.163
nMP / MP	0.962	0.949	0.927
dMP / MP	0.538	0.486	0.293
dMP' / MP	0.698	0.631	0.380

4.4. Discussion

Based on observations during routine clinical practice, it appeared that the design of the EP917 plaques delivered to our center differed from that reported by Astrahan *et al*. and as used in the PS software. Given their disagreement and the lack of literature independently evaluating this type of plaque, we hypothesized that plaque design differences would cause substantial dosimetric differences. The measured slot shape was rounded with rounded ends and had an average depth of 0.46±0.16 mm, which differed significantly from Astrahan *et al*. and the reported depth in the PS software.

When keeping slot length and width fixed and changing the slot depth (consequently moving the seed 0.51 mm farther from the sclera), the dose ratio of dMP/MP by nMP/MP on the CAX at Z=–1 mm (indicative of the maximum outer scleral doses) was 0.306/0.983 or 0.311 (see Table 4.7). For a slot depth change of 0.51 mm, this dose ratio corresponds to –20% per 0.1 mm in slot depth. Conversely, when moving the seed in the opposite direction (*i.e.*, towards the sclera) and keeping the plaque distance fixed, the dose ratio of sMP/MP at the same location was 1.343, for dose change of +35% per 0.1 mm. From the perspective of the DVH outer sclera D_{10} metric (see Table 4.8), these changes were –20**%** per 0.1 mm and +16% per 0.1 mm, respectively, and –11% per 0.1 mm and +2.6% per 0.1 mm for the tumor D_{10} metric, respectively. While the change in slot depth would occur through designs changes to the plaque slots, prevention of the dose increases would require brachytherapy seeds not having dynamic internal components.[31]

Dose results between the 576P plaque and the PS v.5.7.6. TPS results were generally in good agreement, substantially differing only at locations far from the CAX, and may have been due to the approximation of the PS slot in the simulation geometry. Table 4.8 shows that plaque design did not change tumor D_{10} by more than 10% except for dMP and dMP'. When considered in combination with Fig. 4.4f, it is clear that plaque design changes require concern for both relative changes in the dose distribution and absolute changes in delivered dose.

Given the exquisite sensitivity of dose delivery to brachytherapy plaque design, it is crucial that the acceptance testing procedure for eye plaques quantitatively compare the plaque manufacturer specifications for the slot shape, dimensions, and positions on the plaque with measurements performed by the medical physicist preceding clinical use. While dosimetric changes greater than 5% have been observed for plaque design changes of just 0.1 mm, accurate measurements smaller than this value may be too challenging for the majority of clinical medical physicists as their purview in brachytherapy is generally source-strength measurements.[71] Therefore, we suggest that a dimensional tolerance of 0.1 mm used to evaluate such medical devices.

Results of the current study differ from the reference publication by Astrahan *et al*. primarily in slot depth. Astrahan *et al*. reported a depth of 1.4 mm, while our measurements reveal a range of 0.46±0.16 mm (k=1). Given the dramatic difference in results between the MP and dMP plaque designs (even when normalized as in the dMP' case), slot depth (when keeping other aspects fixed, such as slot width and length) is a crucial feature for eye plaques alleging seed collimation. Without proper characterization of the slot (and plaque) geometry, TPS results are not meaningful.

As shown in Table 4.5, Fig. 4.4, and Fig. 4.5, the model EP917 plaque appears to be less conformal than the design used in the PS software. Marwaha *et al*.[48]and Berry *et al*.[55]report favorable clinical results for episcleral brachytherapy. Both publications depict dose distributions for the model EP917 plaque, indicating similar shapes to Fig. 4.4d. Consequently, their clinical findings may be better than reported given the delivered doses were higher than indicated by the TPS results using PS.

With only a single slot loaded, Lesperance *et al*.[72] reported a 2.5 % increase in scleral dose when compared to the same arrangement without slot. A similar result (+3%) was reported by Aryal and Molloy.[73]Lesperance *et al*. compared doses with MC methods to doses expected when using the AAPM TG-43 dose calculation formalism for a fully-loaded round-plaque containing 15 seeds and the 1.4-mm deep slot design by Astrahan *et al*. It appears that Lesperance *et al*. observed this dose ratio to substantially diminish for scleral distances less than 0.4 cm. This observation is supported by their Fig. 7e.

There were several limitations of the current study. The manufacturer did not provide the proprietary composition of the gold-alloy material. Further, the exact slot shape used in PS to perform treatment planning for the model EP917 plaque could not be fully simulated in the current study because of overlap at the slot corners. These limitations were mitigated by evaluating the dosimetric influence of gold-alloy composition and slot design. To keep the current study manageable, only one tumor size and shape was examined with dimensions based on that used in the joint AAPM+ABS TG-129 report.[74] Similarly, the influence of replacing the surrounding water environment with tissue as examined by Lesperance *et al*. was not performed.[72]Another

study limitation was to restrict the dose evaluation metric to D_{10}. While differences among the plaques increased with higher dose, the relative behavior of the different designs did not substantially change for higher dose metrics.

The scope of the current study may be extended with additional research. This would include choosing sources different than the model IAI-125I ^{125}I seed. Another topic would include a comparison between COMS-style plaques and the EP917 plaque to evaluate tumor and scleral doses, as the measured EP917 slot depths were substantially less than reported by Astrahan *et al*.

4.5. Conclusion

Extensive measurements reveal that the slot shape reported by Astrahan *et al*. and the overall plaque design used in the PS software are not representative of the physical devices used for patient treatments. The physical plaques place the seeds in direct contact with the outer sclera and deliver substantially higher doses than indicated by the PS TPS. Radiation transport simulations analyzing dose-distribution sensitivity to plaque design showed that plaques with deeper slots provide superior dose uniformity and homogeneity to the tumor without compromising the scleral dose. A dosimetric analysis on the sensitivity of slot and plaque design revealed that small (i.e., 0.1 mm) physical changes can cause up to 35% changes in dose delivery. Additional research is needed to optimize plaque design and subsequently permit accurate treatment planning and clinical implementation.

American Association of Physicists in Medicine
One Physics Ellipse
College Park, MD 20740-3846
(301) 209-3350
Fax (301) 209-0862
http://www.aapm.org

Office of the Executive Director
Angela R. Keyser
Phone: 301-209-3385 Fax: 301-209-0862
E-mail: akeyser@aapm.org

DATE OF REQUEST: April 21, 2014

FROM:
Mark Rivard
30 Huckleberry Road
Hopkinton, MA 01748

EMAIL ADDRESS: mark.j.rivard@gmail.com

1. **Permission is granted to:**
   Prakash Aryal, Ph.D.
   University of Kentucky

2. **Permission is requested to use the following material:**

   Prakash Aryal, et al., "A modern Monte Carlo investigation of the TG-43 dosimetry parameters for an ^{125}I seed already having AAPM consensus data." Med. Phys. 41, 021702 (2014)

   Prakash Aryal, et al., "Independent dosimetric assessment of the model EP917 episcleral brachytherapy plaque." Med. Phys. (submitted as Manuscript #14-508)

3. **For what purpose:**

   Chapters 3 and 4 of Ph.D. dissertation

Authors seeking permission must also notify the first author of the article from which permission is being sought.

Permission is hereby granted: Angela R. Keyser
Signature

April 23, 2014
Date

The Association's Journals are *Medical Physics* and *Journal of Applied Clinical Medical Physics*
Member Society of the American Institute of Physics and the International Organization of Medical Physics

CHAPTER 5 SUMMARY AND CONCLUSIONS

5.1 Proposed TG-43 Dosimetry Parameters

Existing consensus data (i.e., TG-43 dosimetry parameters) for some brachytherapy sources are based in part on outdated MC codes. The MCNP package has been revised to include updated photon cross-section libraries, variance reduction techniques, and other improvements since its 1987 release. The Advantage^{TM} model IAI-125A ^{125}I brachytherapy seed was selected as a focus of this study.

Air-kerma rates, the dose-rate constant, Λ, radial dose function, $g_L(r)$, and the 2D anisotropy function, $F(r, \theta)$, were calculated for 12 simulation conditions. These parameters were compared with the published literature and TG-43U1S1 consensus data. Results showed that Λ values by Solberg *et al.,* Meigooni *et al*., Taylor and Rogers, and the 2007 AAPM TG-43U1S1 report were 4.3%, 6.2%, 0.3% and 6.3% higher than our Λ value, respectively. The proposed $g_L(r)$ values differed by >10% for r>5 cm compared to Solberg *et al*. and Meigooni *et al.,* respectively. However, the proposed values are within 2% of Taylor and Rogers and within 0.5 % for $0.5 < r < 10$ cm.

F(r,θ) values from our proposed standard were also compared to Solberg *et al.*, Meigooni *et al.*, Taylor and Rogers, and Kennedy *et al*. Large variations were noticed at $\theta < 20°$. At *F (1, 10°),* Solberg *et al.*, Meigooni *et al.* and Taylor and Rogers reported values that were <2%, 37% and 10% higher than our current study respectively.

5.2 Dosimetric Influence of Slot and Plaque Design of the EP917 Eye Plaque

The EP917 plaque was proposed by Astrahan *et al.* These plaques were purported to deliver more conformal and homogeneous doses to the tumor while sparing normal structures, such as the sclera, due to collimation from a deep slot design. But upon acquiring three model EP917 plaques for clinical use, we found that the slots depths and design were different than that described by Astrahan *et al.* and also different than the design within the PS treatment planning software. An investigation was performed to accurately measure the eye plaque slots and overall design to resolve the physical discrepancies. MC methods were used to determine the dosimetric influence of the eye plaque design variations.

Measurements revealed that the slot shape reported by Astrahan *et al*. and the overall plaque design used in the PS software were not representative of the physical devices used for patient treatments. The physical plaques place the seeds in direct contact with the outer sclera and deliver substantially higher doses than indicated by the PS TPS. Radiation transport simulations analyzing dose-distribution sensitivity to plaque design showed that plaques with deeper slots provided superior dose uniformity and homogeneity to the tumor without compromising the scleral dose. A dosimetric analysis of the sensitivity of slot and plaque design revealed that small (i.e., 0.1 mm) physical changes can cause up to 35% changes in dose delivery. Additional research is needed to optimize plaque design and subsequently permit accurate treatment planning and clinical implementation.

5.3 Future work

This work was limited to the EP917 plaque design and ^{125}I (model IAI-125A) seed. Future work of should extend this study to other radionuclide seed models (such as ^{103}Pd and ^{131}Cs) and make quantitative comparisons of the model EP917 plaque with the standardized COMS eye plaques for guiding clinical decision making.

APPENDIX

List of abbreviations

AAPM: American Association of Physicists in Medicine

cGy: centi Gray

COMS: Collaborative Ocular Melanoma Study

HDR: High Dose-Rate

LDR: Low Dose-Rate

MCNP5: Monte Carlo N-particle code, version 5

NIST: National Institute of Standards and Technology

P,E: photons, electrons

P: photons

TG-43: Task Group number 43

TTB: Thick Target Bremsstrahlung

U: Unit of air-kerma strength

USC: University of Southern California

WAFAC: Wide Angle Free Air Chamber

TG43U1: 2004 update to 1995 TG-43 report

BIBLIOGRAPHY

[1] www.cancer.org

[2] www.brachytherapy.com

[3] www.varian.com

[4] M. J. Rivard, B. M. Coursey, L. A. DeWerd, W. F. Hanson, M. S. Huq, G.S. Ibbot, M. G. Mitch, R. Nath, and J. F. Williamson, “Update of AAPM Task Group No. 43 Report A revised AAPM protocol for brachytherapy dose calculations,” Med. Phys. 31(3), 633–674 (2004).

[5] M. J. Rivard, W. M. Butler, L. A. DeWerd, M. S. Huq, G. S. Ibbott, A. S.Meigooni, C. S. Melhus, M. G. Mitch, R. Nath, and J. F. Williamson,“Supplement to the 2004 update of the AAPM Task Group No. 43 Report,” Med. Phys. 34, 2187–2205 (2007).

[6] J. T. Bushberg, J. A. Seibert, E. M. Leidholdt, Jr., and J. M. Boone, The Essential Physics of Medical Imaging, 2nd ed. (Lippincott, Williams, and Wilkins. Philadelphia, (2002), pp. 37

[7] F.H. Attix, Introduction to Radiological Physics and Radiation Dosimetry, (Wiley, New York, 1986), pp. 140.

[8] X-5 Monte Carlo Team.MCNP - A General Monte Carlo N-Particle Transport Code, Version 5, LA-UR-03-1987 (2003).

[9] http//en.wikipedia.org/wiki/Monte_Carlo_method

[10] M. J. Rivard et al., “Update of AAPM Task Group No. 43 Report A revised AAPM protocol for brachytherapy dose calculations,” Med. Phys. 31(3), 633–674 (2004).

[11] http//www.nist.gov/pml/div682/grp02/low-energy-photon.cfm

[12] T.D. Solberg, J. J. DeMarco, G. Hugo, and R. E. Wallace, “Dosimetric parameters of three new solid core I-125 brachytherapy sources,” J. Appl. Clin. Med. Phys. 3, 119 134 (2002).

[13] A. S. Meigooni, J. L. Hayes, H. Zhang, and K. Sowards, “Experimental and theoretical
determination of dosimetric characteristics of IsoAid ADVANTAGE™ 125I brachytherapy source,” Med. Phys. 29, 2152–2158 (2002).

[14] R. Nath, L. L. Anderson, G. Luxton, K. A. Weaver, J. F. Williamson, and A. S. Meigooni, “Dosimetry of interstitial brachytherapy sources Recommendations of the AAPM Radiation Therapy Committee Task Group No. 43,” Med. Phys. 22, 209–234 (1995).

[15] M. J. Rivard, B. M. Coursey, L. A. DeWerd, W. F. Hanson, M. S. Huq, GS. Ibbott, M. G. Mitch, R. Nath, and J. F. Williamson, “Update of AAPM Task Group No. 43

Report A revised AAPM protocol for brachytherapy dose calculations," Med. Phys. 31, 633–674 (2004).

[16] M. J. Rivard, W. Butler, L. A. DeWerd, M. S. Huq, G. S. Ibbott, A.S. Meigooni, C. S. Melhus, M. G. Mitch, R. Nath, and J. F. Williamson, "Supplement to the 2004 update of the AAPM Task Group No. 43 Report," Med. Phys. 34, 2187–2205 (2007).

[17] R. W. Roussin, J. R. Knight, J. H. Hubbell, and R. J. Howerton, Description of the DLC-99/Hugo Package of Photon Interactions, ORNL/RSIC-46, RSIC Data Library Collection, Oak Ridge National Laboratory, Radiation Safety Information Center, 1983.

[18] R. E. P. Taylor and D. W. O. Rogers, "An EGSnrc Monte Carlo-calculated database of TG-43 parameters," Med. Phys. 35, 4228–4241 (2008).

[19] R. M. Kennedy, S. D. Davis, J. A. Micka, and L. A. DeWerd, "Experimental and Monte Carlo determination of the TG-43 dosimetric parameters for the model 9011 THINSeed™ brachytherapy source," Med. Phys. 37, 1681–1688 (2010).

[20] M. J. Rivard, D-A. R. Evans, and I. Kay, " A technical evaluation of the Nucletron FIRST® system Conformance of a remote afterloading brachytherapy seed implantation system to manufacturer specifications and AAPM Task Group report recommendations," J. Appl. Clin. Med. Phys. 6, 22–50 (2005).

[21] http//www.chemicalelements.com/elements/i.html last accessed September 19, 2013.

[22] X-5 Monte Carlo Team, "MCNP – A general Monte Carlo N-Particle transport code, version 5," Los Alamos National Laboratory, Los Alamos, NM (2003).

[23] M. J. Rivard, D. Granero, J. Perez-Calatayud, and F. Ballester, "Influence of photon energy spectra from brachytherapy sources on Monte Carlo simulations of kerma and dose rates in water and air," Med. Phys. 37, 869–876 (2010).

[24] NUDAT 2.6, National Nuclear Data Center, Brookhaven National Laboratory, http//www.nndc.bnl.gov/nudat2/decaysearchdirect.jsp?nuc=125I&unc=nds last accessed September 19, 2013.

[25] J. Pérez-Calatayud, F. Ballester, R. K. Das, L. A. DeWerd, G. S. Ibbott, A. S. Meigooni, Z. Ouhib, M. J. Rivard, R. S. Sloboda, and J. F. Williamson, "Dose calculation for photon-emitting brachytherapy sources with average energy higher than 50 keV Report of the AAPM and ESTRO," Med. Phys. 39, 2904–2929 (2012).

[26] C. S. Melhus and M. J. Rivard, "Approaches to calculating AAPM TG-43 brachytherapy dosimetry parameters for 137Cs, 125I, 192Ir, 103Pd, and 169Yb sources," Med. Phys. 33, 1729–1737 (2006).

[27] M. J. Rivard, “Monte Carlo radiation dose simulations and dosimetric comparison of the model 6711 and 9011 ^{125}I brachytherapy sources,” Med. Phys. 36, 486–491 (2009).

[28] L. T. Dillman and F. C. Van der Lage, Medical Internal Radiation Dosimetry (MIRD) pamphlet 10, 1975.

[29] S. M. Seltzer, P. J. Lamperti, R. Loevinger, M. G. Mitch, J. T. Weaver, and B. M. Coursey, ‘‘New national air-kerma-strength standards for ^{125}I and ^{103}Pd brachytherapy seeds,’’ J. Res. Natl. Inst. Stand. Technol. 108, 337–358 (2003).

[30] L. A. DeWerd. G. S. Ibbott, A. S. Meigooni, M. G. Mitch, M. J. Rivard, K. E. Stump, B. R. Thomadsen, and J. L. M. Venselaar, “A dosimetric uncertainty analysis for photon-emitting brachytherapy sources Report of AAPM Task Group No. 138 and GEC-ESTRO,” Med. Phys. 38, 782–801 (2011).

[31] M. J. Rivard, “Monte Carlo calculations of AAPM Task Group Report No. 43 dosimetry parameters for the MED3631-A/M ^{125}I source,” Med. Phys. 28, 629–637 (2001).

[32] M. J. Rivard, C. S. Melhus, and B. L. Kirk, “Brachytherapy dosimetry parameters calculated for a new ^{103}Pd source,” Med. Phys. 31, 2466–2470 (2004).

[33] J. Katakura, “Nuclear data sheets for A=125,” Nucl. Data Sheets 112, 495–854 (2011).

[34] J. Katakura, “Nuclear data sheets for A=125,” Nucl. Data Sheets 86, 955–1118 (1999).

[35] P. Andreo, D. T. Burns, and F. Salvat, “On the uncertainties of photon mass energy-absorption coefficients and their ratios for radiation dosimetry,” Phys. Med. Biol. 57, 2117–2136 (2012).

[36] J. H. Hubbell, “Photon mass attenuation and energy-absorption coefficients,” Intl. J. Appl. Radiat.Isot.33, 1269–1290 (1982).

[37] G. Luxton and G. Jozsef, “Radial dose distribution, dose to water and dose rate constant for monoenergetic photon point sources from 10 keV to 2 MeV EGS4 Monte Carlo model calculation,” Med. Phys. 26, 2531–2538 (1999).

[38] T. D. Bohm, P.M. DeLuca, Jr., and L. A. DeWerd, “Brachytherapy dosimetry of ^{125}I and ^{103}Pd sources using an updated cross section library for the MCNP Monte Carlo transport code,” Med. Phys. 30, 701–711 (2003).

[39] S. Nag, J. M. Quivey, J. D. Earle, *et al.*, “The American Brachytherapy Society recommendations for brachytherapy of uveal melanomas,” Int. J. Radiat. Oncol., Biol., Phys. **56**, 544–555 (2003).

[40] P. T. Finger, E. R. Simpson, B. Galle, *et al.*, "The American Brachytherapy Society consensus guidelines for plaque brachytherapy of uveal melanoma and retinoblastoma," Brachytherapy **13**, 1–14 (2014).

[41] R. Moore, "Choroidal sarcoma treated by the intraocular insertion of radon seeds," British J. Ophthalmology **14**, 145–156 (1930).

[42] Collaborative Ocular Melanoma Study Group. Ch 12 Radiation therapy. COMS manual of procedures PB95-179693 (National Technical Information Service, Springfield, VA, 1995).

[43] M. Diener-West *et al.*, "The COMS randomized trial of iodine 125 brachytherapy for choroidal melanoma, III Initial mortality findings," Arch. Ophthalmol. **119**, 969–982 (2001).

[44] K. L. Leonard, N. L. Gagne, J. E. Mignano, J. S. Duker, E. A. Bannon, and M. J. Rivard, "A 17-year retrospective study of institutional results for eye plaque brachytherapy of uveal melanoma using ^{125}I, ^{103}Pd, and ^{131}Cs and historical perspective," Brachytherapy **10**, 331–339 (2011).

[45] M. Astrahan, G. Luxton, Q. Pu, and Z. Petrovich, "Conformal episcleral plaque brachytherapy," Int. J. Radiat. Oncol., Biol., Phys. **39**, 505–519 (1997).

[46] S. Nag, D. Wang, H. Wu, C. J. Bauer, R. B. Chambers, and F. H. Davidorf, "Custom-made "Nag" eye plaques for ^{125}I brachytherapy," Int. J. Radiat. Oncol., Biol. Phys. **56,** 1373–1380 (2003).

[47] D. Granero, J. Pérez-Calatayud, F. Ballester, and E. Casal, "Dosimetric study of the 15mm ROPES eye plaque," Med. Phys. **31**, 3330–3336 (2004).

[48] G. Marwaha, A. Wilkinson, J. Bena, R. Macklis, and A. D. Singh, "Dosimetric benefit of a new ophthalmic radiation plaque," Int. J. Radiat. Oncol., Bio., Phys. **84**, 1226–1230 (2012).

[49] L. Zimmermann, A. Amoush, and D. Wilkinson, "Episcleral eye plaque dosimetry comparison for the Eye Physics EP917 using Plaque Simulator and Monte Carlo simulation," Med. Phys. **40**, 309 abstract (2013).

[50] X-5 Monte Carlo Team, "MCNP – A general Monte Carlo N-Particle transport code, version 5," Los Alamos National Laboratory, Los Alamos, NM (2003).

[51] Tables of x-ray mass attenuation coefficients and mass energy-absorption coefficients from 1 keV to 20 MeV for elements Z = 1 to 92 and 48 additional substances of dosimetric interest, National Institute of Standards and Technology.

Available at http//www.nist.gov/pml/data/xraycoef/index.cfm (last accessed April 16, 2014).

[52] NUDAT 2.6, National Nuclear Data Center, Brookhaven National Laboratory, http//www.nndc.bnl.gov/nudat2/decaysearchdirect.jsp?nuc=125I&unc=nds (last accessed April 16, 2014).

[53] M. J. Rivard, "Monte Carlo radiation dose simulations and dosimetric comparison of the model 6711 and 9011 ^{125}I brachytherapy sources," Med. Phys. **36**, 486–491 (2009).

[54] M. J. Rivard, D-A. R. Evans, and I. Kay, "A technical evaluation of the Nucletron FIRST® system Conformance of a remote afterloading brachytherapy seed implantation system to manufacturer specifications and AAPM Task Group report recommendations," J. Appl. Clin. Med. Phys. **6**, 22–50 (2005).

[55] J. L. Berry, S. V. Dandapani, M. Stevanovic, T. C. Lee, M. Astrahan, A. L. Murphree, and J. W. Kim, "Outcomes of choroidal melanomas treated with Eye Physics: A 20 year review," JAMA Ophthalmol. **131**, 1435–1442 (2013).

[56] Personal communication with Wu Liu, Ph.D., Yale University School of Medicine, New Haven, CT, November 20, 2013.

[57] G. J. Kutcher, L. Coia, M. Gillin, *et al*., "Comprehensive QA for radiation oncology," Med. Phys. **21**, 581–618 (1994).

[58] R. Nath, L. L. Anderson, J. A. Meli, A. J. Olch, J. A. Stitt, and J. F. Williamson, "Code of practice for brachytherapy physics Report of the AAPM Radiation Therapy Committee Task Group No. 56," Med. Phys. **24**, 1557–1598 (1997).

[59] J. L. M. Venselaar and J. Pérez-Calatayud, editors. European Guidelines for Quality Assurance in Radiotherapy, Booklet No 8 A practical guide to quality control of brachytherapy equipment. Brussels, Belgium ISBN 90-804532-8 ESTRO (2004).

[60] http//www.dhfco.com/catalog/DHFCat2013.pdf page 24 (last accessed April 16, 2014).

[61] http//people.timezone.com/library/archives/archives631703251272822958 (last accessed April 16, 2014).

[62] http//chemistry.about.com/od/jewelrychemistry/a/goldalloys.htm (last accessed April 16, 2014).

[63] http//www.kayelaby.npl.co.uk/atomic_and_nuclear_physics/4_2/4_2_1.html (last accessed April 16, 2014).

[64] http//www.nist.gov/pml/data/xraytrans/index.cfm (last accessed April 16, 2014).

[65] P. Aryal, J. A. Molloy, and M. J. Rivard, "A modern Monte Carlo investigation of the TG-43 dosimetry parameters for an ^{125}I seed already having AAPM consensus data," Med. Phys. 41, 021702-(1-10)(2014).

[66] M. J. Rivard, "Monte Carlo calculations of AAPM Task Group Report No. 43 dosimetry parameters for the MED3631-A/M ^{125}I source,"Med. Phys. **28**, 629–637 (2001).

[67] http//scien.stanford.edu/pages/labsite/2006/psych221/projects/06/ddpatil/ee362 Project Report.pdf (last accessed April 16, 2014).

[68] http//www.imatest.com/docs/distortion/ (last accessed April 16, 2014).

[69] M. J. Rivard, S-T. Chiu-Tsao, P. T. Finger, A. S. Meigooni, C. S. Melhus, F. Mourtada, M. E. Napolitano, D. W. O. Rogers, R. M. Thomson, and R. Nath, "Comparison of dose calculation methods for brachytherapy of intraocular tumors," Med. Phys. **38**, 306–316 (2011).

[70] C. S. Melhus and M. J. Rivard," COMS eye plaque brachytherapy dosimetry simulations for ^{103}Pd, ^{125}I, and ^{131}Cs," Med. Phys. **35**, 3364–3371 (2008).

[71] W. M. Butler, W. S. Bice, Jr., L. A. DeWerd, J. M. Hevezi, M. S. Huq, G. S. Ibbott, J. R. Palta, M. J. Rivard, J. P. Seuntjens, and B. R. Thomadsen, "Third-party brachytherapy source calibrations and physicist responsibilities Report of the AAPM Low Energy Brachytherapy Source Calibration Working Group," Med. Phys. **35**, 3860–3865 (2008).

[72] M. Lesperance, M. Martinov, and R. M. Thomson, "Monte Carlo dosimetry for ^{103}Pd, ^{125}I, and ^{131}Cs ocular brachytherapy with various plaque models using an eye phantom," Med. Phys. **41**, 031706-(1-13) (2014).

[73] P. Aryal and J. Molloy, "Comparison of dose rates with and without gold backing of USC #9 radioactive eye plaque using MCNP5," Med. Phys. **39**, 3705 abstract (2012).

[74] S-T.Chiu-Tsao *et.al*."Dosimetry of ^{125}I and ^{103}Pd COMS eye plaques for intraocular tumors Report of Task Group 129 by the AAPM and ABS," Med. Phys. **39**, 6161–6184 (2012).

VITA

Prakash Aryal, M.S., DABR

Educational institutions attended and degree awarded:

- 1999 M.S. in Clinical Radiation Therapy Physics, Medical College of Ohio (Currently University of Toledo), Toledo, OH
- 1995 D.R.P (Post-Graduate Diploma in Radiological Physics), Bombay, India
- 1991 M.Sc. in Physics, Tribhuvan University, Kathmandu, Nepal
- 1988 B.Sc. in Physics, Tribhuvan University, Kathmandu, Nepal

Certification:

- American Board of Radiology (ABR), Therapeutic Radiological Physics, 2004.
- OBI Advance Imaging, Varian Medical Systems, 2009.
- Novoste Beta-Cath^{TM} vascular brachytherapy training certificate, 2004.
- Proxima Therapeutics GliaSite^{TM} RTS training certificate, 2003.

Positions held:

Medical Physicist (1999-2000)

Department of Radiation Oncology, Baystate Medical Center, Springfield, MA

Instructor/Clinical Medical Physicist (2000-present)

Radiation Medicine Department, University of Kentucky, Lexington, KY

Director of brachytherapy physics (2011-present)

Radiation Medicine Department, University of Kentucky, Lexington, KY

Abstracts /publications

- **P. Aryal,** J. A. Molloy, and M. J. Rivard, “Independent dosimetric assessment of the model EP917 episcleral brachytherapy plaque,” submitted to Med. Phys. (March, 2014).

- **P. Aryal,** J. A. Molloy, and M. J. Rivard, “A modern Monte Carlo investigation of the TG-43 dosimetry parameters for an ^{125}I seed already having AAPM consensus data,” Med. Phys. 41, 021702-(1-10) (2014).

- **P. Aryal**, J. Molloy, and M. J. Rivard, “Dose distributions for an ^{125}I seed and the USC #9 plaque with design variations," Brachytherapy 13, S97-S98 abstract (2014).

- **P. Aryal**, J A. Molloy, and M J. Rivard “Dosimetry parameters revisited for the IsoAid model IAI-125A brachytherapy seed” Med. Phys.**40**, 286 (2013).

- W. A. Wilson, J. Lacy, R. Cleary, **P. Aryal**, A. Meigooni, R. Rowland, P. Crispen, and W. St. Clair, “Re-implantation of Prostate Brachytherapy Seeds for Salvage Therapy The University of Kentucky Experience,” International Journal of Radiation Oncology biology physics, Volume 87, Issue 2, Supplement , Pages S367-S368, 1 October 2013.

- C. E. Wooten, M. E. Randall, **P. Aryal**, and J. Feddock “Permanent Interstitial Radiation with Cs-131 Implants for Gynecologic Malignancies: Analysis and Results of an Initial 13 Applications.” International Journal of Radiation Oncology biology physics, Volume 87, Issue 2, Supplement, Page S751, 1 October 2013.

- C.E. Wooten, M.E. Randall, **P. Aryal**, J. Feddock, “Low-Dose-Rate (LDR) Interstitial Radiation for Gynecologic Malignancies: A Single Institution Experience.” International Journal of Radiation Oncology biology physics Volume 87, Issue 2, Supplement , Pages S426-S427, 1 October 2013.

- **P. Aryal,** J. A. Molloy, “Comparison of Dose Rates with and Without Gold Backing of USC #9 Radioactive Eye Plaque Using MCNP5” Med. Phys. 39 , 3705 (2012).

- Luo, W; **Aryal, P.,** and Randall M. “Calculation of Prescribed Dose for Permanent Implant with Cs-131 Using LQ Equation including Resensitization”. Med. Phys. 39 , 3811 (2012).

- **P. Aryal,** K. Mittauer, L. Johnson, A. S. Meigooni, and J. A. Molloy “A segmented elongated curvilinear source model for brachytherapy dosimetry,” Brachytherapy 10, S85 abstract (2011).

- W. Luo, M. Young, **P. Aryal**, E J. Johnson, J A. Molloy, “Development of a Quantitative Target Localizing and Tracking Method for IGRT” Med. Phys. 37 , 3153 (2010)

- **P. Aryal,** A. S. Meigooni,“Dose **calculations** around curved elongated Brachytherapy Sources,” Brachytherapy 7, 148 abstract (2009).

- **P. Aryal**, E. Johnson, and A. Meigooni, “Dosimetry of Curvilinear Brachytherapy sources using TG-43U1 Formalism” Med. Phys. 35 , 2727 (2008).

- K. Dou, J. Ashburn, J. Hafendorfer, **P. Aryal**, E. L. Johnson, A. S. Meigooni, R. Zwicker, “Feasibility Study of Parallel-Opposed GRID Therapy Using a Multileaf Collimator” Med. Phys. 35 , 2771 (2008).

- **P. Aryal,** S. Awan, S. A. Dini, A. S Meigooni, and R. Zwicker. “Evaluation of the TG−43 formalism for dose calculations around curvilinear brachytherapy sources,” Brachytherapy 8, 169-170 abstract (2008).

- K. Dou, J. Hafendorfer, **P. Aryal**, J. Ashburn, E. Johnson, A. Meigooni, R. Zwicker, “Therapeutic advantage of GRID therapy using a multileaf collimator.” Med. Phys. 34 , 2498 (2007).

- K. Dou, J. Ashburn, **P. Aryal**, E. Johnson, and R. Zwicker “Therapeutic advantage of GRID therapy for a single high dose fraction using a multileaf collimator.” ICRR2007.

- **P. Aryal**, J. Ashburn “Loss of Beam Flatness Due to the Double Penumbra Effect in Closely Collimated Electron Applicators and Consideration Selecting Oversized Applicators,” Presented at the American Association of Physicists in Medicine (AAPM) meeting July 14-July 18, 2002.

- E.I. Parsai, K.M Ayyangar, **Aryal, P**., S. Malik, and J.J. Feldmeier,“A Procedural Menu to Start a Thermoluminescent Dosimetry (TLD) Program For Clinical Applications”; Med Phys. 26-6 1054, 1999.

- K.M. Ayyangar, Parsai, E.I., **Aryal, P.,** Malik, S., and Feldmeier, J.J.; “A Computer Technique for Independent Hand Calculation of the High Dose Rate (HDR) Brachytherapy Dose Using VariSource Cadplan BT Data, Expanding it to 3-D Dose Surface and Combining With External Beam Dose.” Med Phys. 26-8 1845, 1999.

- “Clinical and Physical Aspects of Cancer of Larynx” Presented at seminar conducted by Bhabha Atomic Research Center, India for Post Graduate Diploma in Radiological Physics Students in September 1995.

- “Clinical and Physical Aspects in Radiotherapy” Presented at 3rd international oncology conference at Tribhuvan University Teaching Hospital, September 21-23, 1996, Nepal.